# Annual carbon emissions from land-use change in China from 1000 to 2019

Fan Yang[1,2], Guanpeng Dong[1,2], Xiaoyu Meng[1,2], Richard A. Houghton[3], Yang Gao[1,2], Fanneng He[4], Meijiao Li[5], Wenjin Li[1], Zhihao Liu[1], Xudong Zhai[1], Pengfei Wu[1], Hongjuan Zhang[1,2], Qinqin Mao[6], Yuanzhi Yao[7], Bing Li[1], Chao Yue[8]

[1]Key Research Institute of Yellow River Civilization and Sustainable Development, Henan University, Kaifeng 475001, China

[2]Laboratory of Climate Change Mitigation and Carbon Neutrality, Henan University, Zhengzhou 475001, China

[3]Woodwell Climate Research Center, Falmouth, MA 02540, USA

[4]Key Laboratory of Land Surface Pattern and Simulation, Institute of Geographic Sciences and Natural Resources Research, Chinese Academy of Sciences, Beijing 100101, China

[5]College of Resources and Environment, Shanxi University of Finance and Economics, Taiyuan 030006, China

[6]Piesat Information Technology Co., Ltd., Xian, 710100, China

[7]School of Geographic Science, East China Normal University, Shanghai, 200241, China

[8]College of Natural Resources and Environment, Northwest Agriculture and Forestry University, Yangling 712100, China

*Correspondence to:* Guanpeng Dong (gpdong@vip.henu.edu.cn), Fanneng He (hefn@igsnrr.ac.cn), and Chao Yue (chaoyue@ms.iswc.ac.cn)

**Abstract.** Long-term land-use changes have a profound impact on terrestrial ecosystems and the associated carbon balance. Current estimates of China's historical carbon emissions induced by land-use change vary widely. For example, from 1950 to 2021, the magnitude of variations in China exhibited great uncertainty, with global estimates reaching a relative uncertainty of 150%, while over the past 300 years, national-scale estimates showed a relative uncertainty of 102%. Here, current mainland China was taken as the study area, and the 32 provincial units (excluding Macao and Hong Kong) were merged into 25 regions. We utilized a bookkeeping method to quantify China's annual carbon budget resulting from land-use change between 1000 and 2019, driven by a millennial dataset of land-use change in China at provincial level, assisted by comprehensive soil and vegetation carbon density datasets. This approach, which was supported by high-confidence land-use change data, a comprehensive carbon density database compiled from over 10,000 existing field samples, and the latest published disturbance-response curves, enhanced the accuracy of carbon budget estimates. The results revealed that cumulative carbon emissions from land-use change in China reached 19.61 Pg C over the past millennium. Moreover, critical turning points occurred in the early 18$^{th}$ century and early 1980s, with emissions accelerating in the 18$^{th}$ century and transitioning from carbon source to carbon sink in the early 1980s. Our findings revealed that the values were 68%–328% higher than the previous 300-year estimates, suggesting that historical carbon emissions from land-use change in China may have been significantly underestimated. This study provides a robust historical baseline for assessing both present and future terrestrial ecosystem carbon budgets at national and provincial scales. The dataset is available at https://doi.org/10.5281/zenodo.14557386 (Yang et al., 2025).

## 1 Introduction

Carbon fluxes from historical and current land-use change, including both gross emissions and sinks, globally constitute a net carbon source and represent a critical component of the global carbon budget (Houghton and Nassikas, 2017). Reversing land use practices that cause emissions can provide insights into the potential of land management to remove carbon from the atmosphere. Improved quantification of the carbon dynamics associated with land-use change is hence needed to provide a better understanding of the global carbon cycle and the future carbon sink potential of terrestrial ecosystems (Friedlingstein et al., 2023; Obermeier et al., 2024).

Although the estimated contemporary carbon emissions from land-use change account for only 10–15% of anthropogenic carbon emissions (Friedlingstein et al., 2022; Friedlingstein et al., 2020), their historical contributions were much higher. Land-use change has been estimated to contribute nearly 20 ppm to current atmospheric $CO_2$ concentrations, with this contribution dating back at least 1,000 years (Pongratz et al., 2009). Over the past 150 years, carbon emissions from land-use change have accounted for up to 33% of global anthropogenic carbon emissions (Houghton et al., 2012). Recent carbon accounting has shown that since 1750, land-use change has been a major source of $CO_2$ emissions, accounting for 54% of the cumulative $CO_2$ emissions from 1750 to 2020, with fossil fuel $CO_2$ emissions not surpassing those from land-use change until the mid-1960s (Dorgeist et al., 2024; Wedderburn-Bisshop, 2024). Furthermore, historical carbon emissions from land-use change provide crucial insights into how the global carbon cycle responds to environmental changes (Houghton and Castanho, 2023; Yue et al., 2020; Houghton and Nassikas, 2017).

Given the profound impact of land-use change, particularly over long timescales, numerous studies have focused on long-term global estimates of carbon emissions from land-use change (Houghton and Castanho, 2023; Mendelsohn and Sohngen, 2019; Houghton and Nassikas, 2017; Kaplan et al., 2011; Pongratz et al., 2009). However, uncertainties persist in these estimates (Winkler et al., 2023), with net land-use change carbon fluxes exhibiting the highest relative uncertainty in global carbon budget assessments (Friedlingstein et al., 2022). These uncertainties arise not only from differences in estimation models, parameters, and carbon density datasets but also from historical land-use change data. In particular, reliable land-use change datasets prior to the mid-20th century are often lacking for many countries, including China.

One typical approach to reconstructing historical land-use change is to use historical population data as a proxy combined with linear backcasting (Pongratz et al., 2008; Klein Goldewijk, 2001; Ramankutty and Foley, 1999). Although this method works reasonably well for estimating cropland and pasture areas, it is less suitable for calculating changes in forest cover, which has a high impact on estimated terrestrial ecosystem carbon budgets because of the higher carbon densities of forest ecosystems relative to that of cropland or grassland. As a result, researchers often subtract the area of cropland and pasture from the potential natural vegetation to estimate forest cover change (Hurtt et al., 2020; Klein Goldewijk et al., 2017; Pongratz et al., 2008; Ramankutty and Foley, 1999). However, this approach fails to capture large-scale forest cover change

driven by factors such as shifting cultivation, timber and fuel demand in addition to land conversion for agriculture. Consequently, this indirect method can only reflect the conversion relationship among forests, croplands, and pastures and thus often underestimates the actual extent of historical forest change. Therefore, linear backcasting or potential vegetation subtraction often introduce great uncertainties (Kabora et al., 2024; Yang et al., 2020; He et al., 2018) that are carried over into land-use carbon emission estimates.

China has a vast territory and a long history of land use, making it an important contributor to global terrestrial carbon dynamics caused by anthropogenic land-use change and land management. Although most global and regional studies on land-use change focus on the post-industrial era or the past three centuries, China's intensive and extensive land-use activities date back at least a millennium, thus representing a unique historical trajectory (He et al., 2025, 2023). From approximately AD 1000 (coinciding with the Northern Song Dynasty), ecological degradation in China showed a marked rise. This degradation was manifested through multiple pathways: accelerated erosion on the Loess Plateau, recurrent floods in the lower Yellow River Basin, large-scale lake siltation and disappearance in northern China, and progressive soil erosion coupled with natural vegetation loss in the southern hill regions (Wu et al., 2020; Chen et al., 2012). Such millennial-scale land-use transitions would have generated substantial carbon emissions, particularly from deforestation. However, the relatively stable pre-industrial global $CO_2$ concentrations likely obscured these regionally significant anthropogenic carbon fluxes because localized emissions in areas such as China could have been offset by concurrent carbon sinks elsewhere. Additionally, the full trajectory or specific stages of historical land-use change in China can serve as a "historical analogue" for other developing countries. For many countries and regions, systematically revealing the processes and mechanisms of land-use change and associated carbon emissions—driven by long-term population growth and policy shifts—can help overcome the limitations associated with a lack historical records and reliance on static assumptions.

China has abundant historical documentation from a number of dynasties, such as tax records for cropland areas. Scholars have used these records to reconstruct long-term, high-confidence datasets of cropland areas, thereby providing a strong foundation for estimating historical land-use change carbon emissions. Previous studies have extensively reconstructed historical land use across China and specific regions (He et al., 2023; Jia et al., 2023; Wei et al., 2022; Yang et al., 2022; Yu et al., 2021; Li et al., 2016; Ye et al., 2009), as well as the associated carbon emissions (Yang et al., 2023; Yu et al., 2022; Yang et al., 2019; Li et al., 2014; Ge et al., 2008; Houghton and Hackler, 2003). However, existing estimates vary widely and exhibit great uncertainty. For example, estimates of cumulative net carbon emissions from land-use change in China from 1950 to 2021 based on three internationally recognized bookkeeping models exhibited a relative uncertainty of up to 150% (ratio of the standard deviation to the mean estimate) (Obermeier et al., 2024). Moreover, independent estimates of carbon emissions from land-use change over the past 300 years for China also showed a relative uncertainty of 102% (Yang et al., 2023; Yang et al., 2019; Ge et al., 2008; Houghton and Hackler, 2003). Although uncertainty can be reduced by improving model selection and parameters, highly reliable land-use change data remain crucial (Dorgeist et al., 2024; Yu et al., 2022).

To address these issues, this study combined several locally reconstructed, high-confidence, long-term land-use change datasets with comprehensive carbon density datasets to estimate carbon emissions from land-use change for 1000–2019 in China. First, we extended the analysis period from 1700 to 1980 to 1000 to 2019 using newly published millennial land-use change reconstruction data for China (He et al., 2023; He et al., 2024) in combination with data from the Second and Third National Land Surveys in China. This update also improves the reliability of the data, thus providing more confident historical land-use change trajectories and effectively reducing the uncertainty in carbon budget estimates. Second, we developed new land-use conversion rules that clarify the attribution of deforestation beyond conversion to cropland, which is an essential component for calculating annual land-use change rates. Third, carbon density sampling data were enriched to enhance their representativeness. Finally, a bookkeeping model with the latest published disturbance-response curve was used to calculate the annual carbon fluxes associated with long-term land-use change in China. This method represents a key approach used by both the IPCC and Global Carbon Project (GCP) to estimate carbon emission fluxes from land-use change.

## 2. Material and methods

### 2.1 Study area

China's territorial and administrative boundaries have changed frequently over the past millennium, with the country experiencing a succession of different regimes, including the Liao, Song, Jin, Yuan, Ming, and Qing dynasties, the Republic of China, and the People's Republic of China (Fig. 1a–e). To facilitate the alignment of data across different historical periods, this study used the current land area of mainland China as the study region and adopted the territorial and administrative coordination scheme proposed by He et al. (2023) (Fig. 1f), in which the 32 provincial units (excluding Macao and Hong Kong) were merged into 25 regions. This coordination scheme also serves as a fundamental spatial unit for historical land-use change data in China (cropland, forest, and grassland).

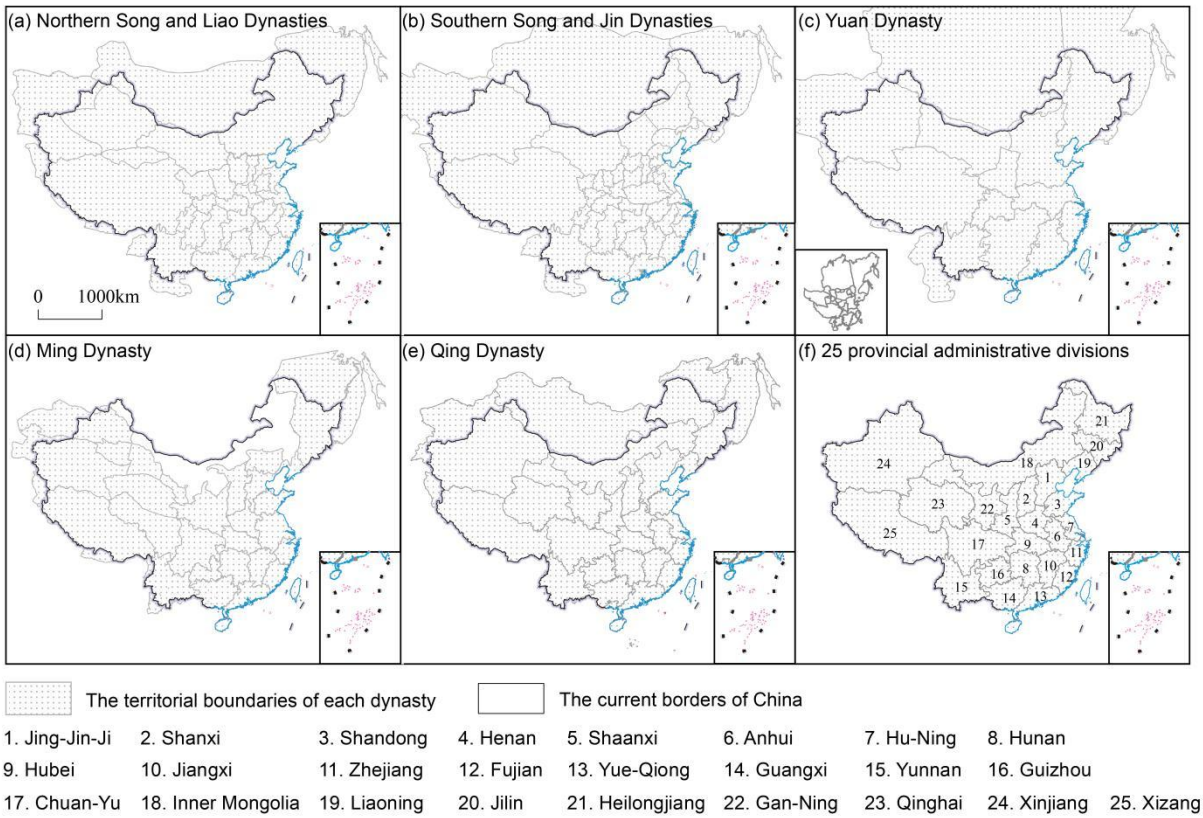


**Figure 1.** Territorial changes across dynasties and the 25 merged provincial-level administrative divisions of China. The following provincial-level administrative regions were merged: Beijing, Tianjin, and Hebei were merged into JingJin-Ji (No.1); Shanghai and Jiangsu were merged into Hu-Ning (No.7); Guangdong and Hainan were merged into Yue-Qiong (No.13); Sichuan and Chongqing were merged into Chuan-Yu (No.17); and Gansu and Ningxia were merged into Gan-Ning (No.22). Due to data limitations, this study did not include Taiwan Province. Maps in panels (a)–(e) were obtained from the Historical Atlas of China (Tan, 1982).

### 2.2 Data sources

This study used two main types of data: long-term land-use data (cropland, forest, and grassland) and carbon density data (vegetation carbon density and soil carbon density).

#### 2.2.1 Land-use data

Land-use data for the period 1000–2019, covering 131 time points, included both historical reconstruction data and survey-based statistics. For the period 1000–1999, provincial cropland data for China were obtained from several previous studies (Table 1). These data were primarily reconstructed for cropland areas using tax records in historical archives dating back to the Northern Song Dynasty (Yang et al., 2024; Li et al., 2020; Li et al., 2018a; Li et al., 2018b; Li et al., 2016; Ge et al., 2004). Provincial forest data for 1000–1998 were sourced from He et al. (2024, 2017, 2008) (Table 1) and are referenced to as historical deforestation data. Provincial grassland data for 1000–2000 were also obtained from He et al. (2024) (Table 1).

**Table 1.** Data sources for land-use change in China

| Data variables | Temporal coverage | Spatial resolution | Data type | Data source/ Reference |
|---|---|---|---|---|
| Cropland | 1000, 1066, 1078, 1162, 1215 | Province | Reconstruction | He et al. (2017); Li et al. (2018a) |
| | 1102 | Province | Reconstruction | Yang et al. (2024) |
| | 1290 | Province | Reconstruction | Li et al. (2018b) |
| | 1393, 1583, 1620 | Province | Reconstruction | Li et al. (2020) |
| | 1661–1949 (21 time points) | Province | Reconstruction | Ge et al. (2004) |
| | 1949–1999 (27 time points) | Province | Statistics | Li et al. (2016) |
| Forest | 1000–1949 (50-year interval) | Province | Reconstruction | He et al (2024) He et al (2008) |
| | 1962, 1976, 1981, 1988, 1993, 1998 | Province | Statistics | He et al (2015) |
| Grassland | 1000, 1100, 1200, 1300, 1400, 1500, 1600, 1700, 1800, 1900, 2000 | Province | Reconstruction | He et al (2024) |

This study used survey-based data from the Second National Land Survey (2009) and Third National Land Survey (2019) (Appendix Table A1) for the period after 2000. These surveys, conducted by the Chinese government, are considered highly credible. As large-scale national projects directed by the Chinese government, these surveys involved extensive, multi-year efforts and were subject to rigorous quality control throughout the entire process, ensuring their high credibility.

The 25 provinces shown in Fig 1 were used as spatial units for historical land-use data in China. Cropland, forest, and grassland data from the national land survey reports were adjusted according to this scheme to ensure consistency.

### 2.2.2 Overview of long-term land-use change data

Unlike modern geographic elements, which can be verified through techniques such as sample collection, field surveys, and remote sensing monitoring, historical land-use change data spanning long periods and large regions are difficult to independently validate because of temporal and spatial constraints. Our data encompass three land-use types: cropland, forest, and grassland, derived from multiple published studies. The reliability of these data is assessed through the examination of data sources, the rationality of the estimation or reconstruction methods, and the degree to which the results align with expert knowledge. Their quantitative changes (expansion and contraction) are consistent over the time series and have been cross-validated against population trends, dynastic policies, and documented historical events. Based on these data, we designed land-use conversion rules (Section 2.3.2) to integrate the independently reconstructed historical data of different land-use types. This integrated data were then used to drive subsequent carbon budget calculations. Historical land-use data for China from global datasets are known to have poor support from local expert knowledge and thus failed to capture more recent land-use dynamics (Yu et al., 2022). For this reason, we utilized regionally reconstructed historical land-use change data for China. We argue that the latter provides a more reliable representation of land-use trajectories in China over the past

millennium. Below we further detail the rationale behind this choice.

The historical cropland data used in this study is typical examples of regionally reconstructed data. Historically, China has been a major agricultural nation, with agriculture forming the primary pillar of socioeconomic development in ancient Chinese society. Cropland area directly influences agricultural tax revenues, and as a result, tax records for cropland areas have been extensively documented in the historical literature, making them highly reliable accounts of cropland area. Furthermore, although these records may not precisely correspond to actual cropland, scholars have developed conversion mechanisms to convert tax records to actual cropland area across different historical periods. These methodologies have been used to reconstruct cropland areas over various periods (Yang et al., 2024; Li et al., 2020; Li et al., 2018a; Li et al., 2018b; Li et al., 2016; Ge et al., 2004) and the results have been peer-reviewed and published to ensure the reliability of the data sources, methods, and processes. Although global historical land-use datasets (such as the HYDE 3.2 dataset) have partly incorporated these regional reconstructions to reflect historical cropland changes at the national level for China, they are prone to error at provincial scale. Detailed analyses and assessments of the provincial errors in the global datasets have been performed by Zhao et al. (2022) and Fang et al. (2020).

Historical records of the forests in China are mainly scattered in various historical texts. While quantitatively reconstructing forest cover change based solely on literary sources is challenging, qualitative descriptions can be successfully generated. Accordingly, several key features of forest changes in China over time have been revealed: (1) northern China has a long history of deforestation and as early as a thousand years ago, forests in the North China Plain were already nearly depleted; (2) over the following millennium, deforestation gradually expanded from plains and hills to mountainous areas; and (3) the deforestation process started from around the middle and lower reaches of the Yellow River and gradually extended to the middle and lower reaches of the Yangtze River, and then to the southern coastal areas of China, Southwest China, and Northeast China. These features provide crucial evidence for assessing the reliability of reconstructed forest data. By constructing a non-linear “inverted S-shaped” relationship between forest cover change and population size data, historical forest area changes used in this study were estimated based on qualitative records of deforestation in Chinese history (He et al., 2024). The “inverted S-shaped” curve reflects the dynamic relationship between historical population size and deforestation. In the early stages, when the population is relatively small, forest resources are plentiful and the rate of deforestation remains slow. As the population grows, deforestation accelerates rapidly, resulting in a significant loss of forest cover. Eventually, despite the population continuing to increase, the scarcity of remaining forests causes the rate of deforestation to slow down. In contrast, global historical land-use datasets depict historical forests in China by subtracting the area of cropland and pasture from the potential forest vegetation area in each grid cell simulated by vegetation modeling. Therefore, this approach primarily reflects the transition of forest cover to human land-use and fails to accurately capture other factors that influence forest area changes, such as fuelwood and timber consumption. For a detailed evaluation of historical forest data in global datasets for China, please refer to Yang et al. (2020).

For historical changes in grassland area, global datasets such as HYDE (Klein Goldewijk et al., 2017), SAGE (Ramankutty and Foley, 1999), and PJ (Pongratz et al., 2008) have been generated based on the FAO's definition of pasture. However, Chinese scholars use the plant geography definition of grassland. This conceptual difference is one of the major reasons for the large discrepancies in grassland area for China between global datasets and the reconstructions generated by Chinese scholars (He et al., 2018). Unlike Europe and North America, where climate-driven land-use patterns for livestock (grassland) dominate, China (especially in the eastern regions) has historically developed a cropland-based husbandry system under a monsoon climate and a relatively smaller-scale grassland agriculture system. Therefore, global datasets based on European and North American land-use practices, which use historical population and per capita pasture area as proxies to derive pasture or grassland data, are not applicable to China. For an evaluation of historical grassland data for China in global datasets, refer to He et al. (2018). Moreover, historical grassland cover data used in He et al. (2024) are based on historical cropland and forest data. These historical data consider the occupation of grassland by cropland expansion in western and northern China and also reflect the dynamic relationship between deforested land and secondary grasslands in eastern and southern China.

Overall, the long-term land-use data used in this study were based on historically reconstructed data rather than retrospective simulation data, with independent reconstructions performed for historical cropland and forest data (Yang et al., 2024; He et al. 2024, 2017, 2008; Li et al., 2020, 2018a, 2018b, 2016; Ge et al., 2004). Consequently, these reconstructed data are closer to historical facts and provide unique value for assessing the environmental effects of long-term human land-use changes.

### 2.2.3 Carbon density data

This study compiled and harmonized a provincial soil and vegetation carbon density dataset for China, integrating 10,424 sample points from multiple major sources. Soil carbon density data were derived from the following three sources. (1) The 2010s China Land Ecosystem Carbon Density Dataset (Xu et al., 2019). This dataset consolidates field measurement data from 2004 to 2014 reported in publicly available literature. From this dataset, 1,235 sample points for forest soil carbon density and 614 sample points for grassland soil carbon density were extracted. (2) The Second National Soil Survey of China (1979–1985). This survey resulted in the publication of the Soil Chronicles Atlas of China, Volumes 1–6, which record soil property data from the 1980s. From this, 339 sample points for forest soil properties and 147 sample points for grassland soil properties were extracted. (3) The Chinese Soil Series (since 2008). This investigation produced the Soil Series Atlas of China, which consists of 30 volumes (Appendix Table B1). From this dataset, 724 and 529 sample points for forest and grassland soil properties were extracted, respectively. The spatial distribution of the sample points is presented in Appendix Fig. B1.

The results of the two large-scale soil surveys were documented in books that recorded soil properties during different periods in China. This study extracted information from these surveys, including the geographic location (latitude and longitude), soil depth (0–100 cm), soil type, organic carbon content, soil bulk density, and >2 mm gravel content, and applied Eq. (1) to calculate the soil carbon density. The formula used to calculate soil carbon density based on soil properties is as follows:

$$C_S = \sum_{i=1}^{n} SOC_i \times D_i \times BD_i \times (1-SC_i) \times 0.1 \quad (1)$$

where $C_S$ is the soil organic carbon density, $SOC_i$ is the organic carbon percentage in the $i$-th soil layer (%), $D_i$ is the thickness of the $i$-th soil layer (cm), $BD_i$ is the bulk density of the $i$-th soil layer (g/cm³), $SC_i$ is the percentage of gravel (>2mm) in the $i$-th soil layer (%), and $n$ is the number of layers in the 100 cm soil profile. This study only selected sample points with a soil profile thickness of $\geqslant$ 100 cm and considered only the carbon density within the top 100 cm was considered. For sample points lacking bulk density data, bulk density was estimated using an empirical transfer function from Yang et al. (2007). This function is based on the negative correlation between bulk density (BD, g/cm$^3$) and soil organic matter (SOM, %) , with the specific formula:

$$BD = 0.29 + 1.2033 \times e^{-0.0775 \times SOM} \quad (2)$$

Vegetation biomass carbon density data were sourced from the 2010s China Land Ecosystem Carbon Density Dataset (Xu et al., 2019), including carbon density data from both aboveground (forests: 1,610 points, grasslands: 2,224 points) and belowground layers (forests: 1,544 points, grasslands: 1,458 points) of forest and grassland ecosystems. The formula for calculating vegetation carbon density is as follows:

$$C_V = C_{above\_ground} + C_{below\_ground} \quad (3)$$

where $C_V$ is the vegetation biomass carbon density, $C_{above\_ground}$ is the aboveground vegetation carbon density, and $C_{below\_ground}$ is the belowground vegetation carbon density.

The collected vegetation biomass and soil carbon density data were grouped according to the 25 merged province-level administrative divisions described above based on the geographic coordinates of the data points. Overall, for each province, the sample points exhibited a normal distribution (Appendix Figs. B2–B4). The arithmetic mean was used to calculate the provincial-level average carbon density. For provinces with exceptionally high or low values, the median was used to reflect the average carbon density and minimize the influence of outliers. The provincial-level vegetation and soil carbon density data are listed in Table 2.

**Table 2.** Provincial vegetation and soil carbon density data

| Code | Province/region | Forest (Mg/ha) | | Grassland (Mg/ha) | |
|---|---|---|---|---|---|
| | | SOCD | VCD | SOCD | VCD |
| No.1 | Jing-Jin-Ji | 75.39 (n=104) | 43.83 (n=117) | 88.32 (n=53) | 7.61 (n=19) |

| | | | | | |
|---|---|---|---|---|---|
| No.2 | Shanxi | 59.98 (n=65) | 40.63 (n=66) | 56.13 (n=115) | 8.77 (n=71) |
| No.3 | Shandong | 60.42 (n=30) | 42.29 (n=26) | / | / |
| No.4 | Henan | 59.03 (n=17) | 42.41 (n=24) | / | / |
| No.5 | Shaanxi | 74.29 (n=174) | 29.78 (n=101) | 64.75 (n=110) | 4.03 (n=45) |
| No.6 | Anhui | 86.90 (n=44) | 63.06 (n=57) | / | / |
| No.7 | Hu-Ning | 91.79 (n=31) | 37.63 (n=27) | / | / |
| No.8 | Hunan | 92.60 (n=174) | 51.94 (n=42) | / | / |
| No.9 | Hubei | 139.57 (n=63) | 48.00 (n=20) | / | / |
| No.10 | Jiangxi | 93.29 (n=162) | 50.81 (n=44) | / | / |
| No.11 | Zhejiang | 115.13 (n=69) | 54.14 (n=35) | / | / |
| No.12 | Fujian | 117.71 (n=114) | 58.80 (n=72) | / | / |
| No.13 | Yue-Qiong | 111.36 (n=233) | 37.33 (n=92) | / | / |
| No.14 | Guangxi | 108.26 (n=156) | 55.87 (n=105) | 99.32 (n=17) | / |
| No.15 | Yunnan | 105.84 (n=110) | 76.26 (n=67) | 100.52 (n=14) | / |
| No.16 | Guizhou | 129.37 (n=64) | 50.31 (n=29) | 284.18 (n=35) | / |
| No.17 | Chuan-Yu | 98.83 (n=132) | 55.96 (n=159) | 143.09 (n=50) | 1.25 (n=142) |
| No.18 | Inner Mongolia | 69.38 (n=179) | 41.60 (n=263) | 88.79 (n=119) | 5.77 (n=416) |
| No.19 | Liaoning | 91.13 (n=70) | 44.74 (n=43) | 77.71 (n=35) | 3.32 (n=25) |
| No.20 | Jilin | 95.09 (n=57) | 73.85 (n=39) | 67.09 (n=30) | 3.06 (n=24) |
| No.21 | Heilongjiang | 145.45 (n=91) | 64.63 (n=114) | 93.58 (n=28) | 2.98 (n=22) |
| No.22 | Gan-Ning | 99.44 (n=88) | 36.80 (n=57) | 54.66 (n=236) | 3.80 (n=159) |
| No.23 | Qinghai | 75.87 (n=20) | 30.54 (n=36) | 108.60 (n=249) | 6.45 (n=385) |
| No.25 | Xinjiang | 64.32 (n=22) | 25.59 (n=42) | 93.97 (n=119) | 4.09 (n=91) |
| No.24 | Xizang | 129.33 (n=35) | 82.43 (n=20) | 58.89 (n=167) | 4.20 (n=291) |

SOCD refers to soil organic carbon density, VCD refers to vegetation carbon density.

250

### 2.3 Methods

Annual emissions of carbon from land-use change were calculated with a bookkeeping model based on two types of data: rates of land-use change and per hectare effects of land-use change on carbon stocks (Fig. 2). The former was calculated by constructing land-use transition rules, while the latter was derived from the disturbance response curves in the bookkeeping
255 model, combined with provincial vegetation and soil carbon density datasets. Due to data limitations, this accounting does not consider carbon emissions from wood harvesting.

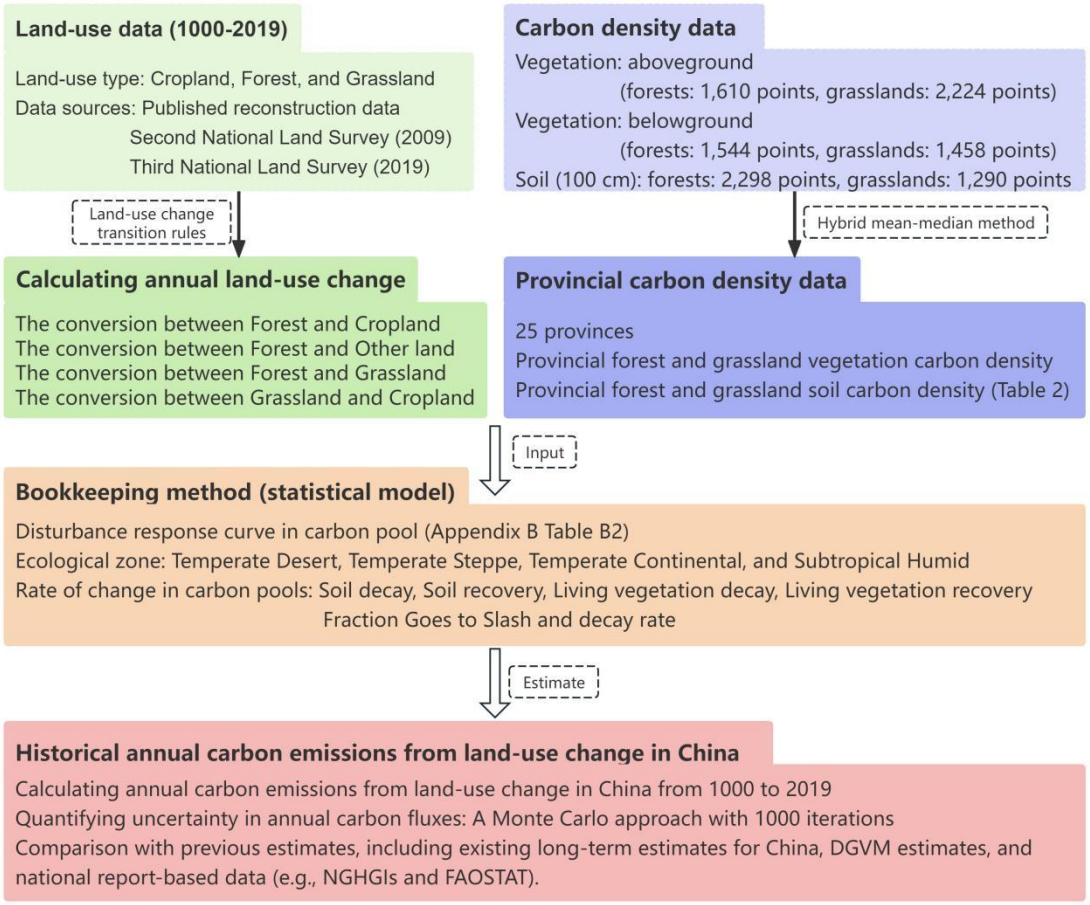


**Figure 2.** Framework for calculating annual carbon emissions based on the bookkeeping model. The color scheme delineates the framework's primary modules: data inputs for land use (green) and carbon density (blue), the core bookkeeping model (orange), and the final results and analysis of carbon emissions (red).

### 2.3.1 Bookkeeping method

The bookkeeping method (a statistical model) proposed by Houghton and Castanho (2023) was employed to estimate the annual carbon emissions caused by land-use changes in China from 1000 to 2019. Due to data limitations, long-term historical land-use reconstructions in China are primarily constrained to land-use "states" (e.g., total cropland or forest area at national/provincial levels for specific years) rather than spatially explicit land-use transitions. This characteristic, combined with the provincial-level spatial resolution of our data, makes such reconstructions inherently compatible with the bookkeeping model adopted here (Houghton and Castanho, 2023). Bookkeeping is widely used to estimate carbon emissions across multiple spatial and temporal scales and characterizes the impacts of human-induced land-use changes on carbon stocks in vegetation and soil across various terrestrial ecosystems (Qin et al., 2024; Yang et al., 2023; Bastos et al., 2021; Hartung et al., 2021). The bookkeeping model used in this study is primarily driven by land-use change data and utilizes observed vegetation and soil carbon density data and specific disturbance response curves for each land-use transition type. As this method excludes the influence of unchanged land-use types and environmental changes, such as carbon dioxide

concentrations and climate change, it quantifies direct anthropogenic fluxes and ignores carbon fluxes driven by environmental changes (Dorgeist et al., 2024; Houghton and Castanho, 2023). Consequently, the results of this method are frequently incorporated into global carbon budget estimates (Friedlingstein et al., 2023).

Our bookkeeping model uses statistical data rather than spatial grid data as input and calculates the net carbon change in terrestrial ecosystems due to land-use changes on an annual basis. The disturbance response curves specify the dynamic changes in carbon pools following land-use transition, including biomass (both aboveground and belowground), litter (branches, trunks, roots, etc.), and soil organic carbon pools over time for each land-use type and per hectare of land-use change until a new carbon density equilibrium is reached (Houghton and Castanho, 2023). The response time for carbon release or absorption due to land-use changes can range from decades to centuries. The values of the disturbance response curves (*f*) were derived from Houghton and Castanho (2023) (see Appendix B Table B2). Therefore, the carbon emission flux estimated at any given time includes both instantaneous and legacy fluxes from previous land-use changes. The calculation formula is as follows:

$$\Delta C_{flux}(j, t)=\sum_{k}\left(R_{LU}(j, k, t)\times C_{v}(j)\times f_{vge}\right)+\left(R_{LU}(j, k, t)\times C_{s}(j)\times f_{soil}\right)+\left(R_{LU}(j, k, t)\times C_{v}(j)\times f_{slash}\right) \quad (4)$$

where $\Delta C_{flux}(j, t)$ is the carbon emission flux due to land-use change in province $j$ at time $t$, $R_{LU}(j, k, t)$ is the land-use transition amount for type $k$ in province $j$ at time $t$, $C_V(j)$ and $C_s(j)$ are the vegetation and soil carbon densities in province $j$, respectively, and $f$ is the disturbance response curve for vegetation and soil carbon pools.

### 2.3.2 Calculating annual land-use change

The high-confidence, long-term land-use data compiled for China, specifically the cropland, forest, and grassland data, do not cover all land types. Therefore, this study refers to the land-use types used in the carbon emission estimation by Houghton and Castanho (2023) and major land-use types listed in the FAO (2021) report. Following the approach outlined by Houghton and Castanho (2023), we classified land types other than these three as “other land”, thus defining four land-use categories: cropland, forest, grassland, and other land. The first three land-use types were derived from reconstructed data and survey statistics, as shown in Fig. 3 and Table 1. The “other land” category refers to the residual area in a province after excluding cropland, forest, and grassland, and it encompasses all land types not covered by the three primary land-use categories. Compared with contemporary land-use classification standards, our “other land” category includes a variety of both human-affected and unaffected land types.

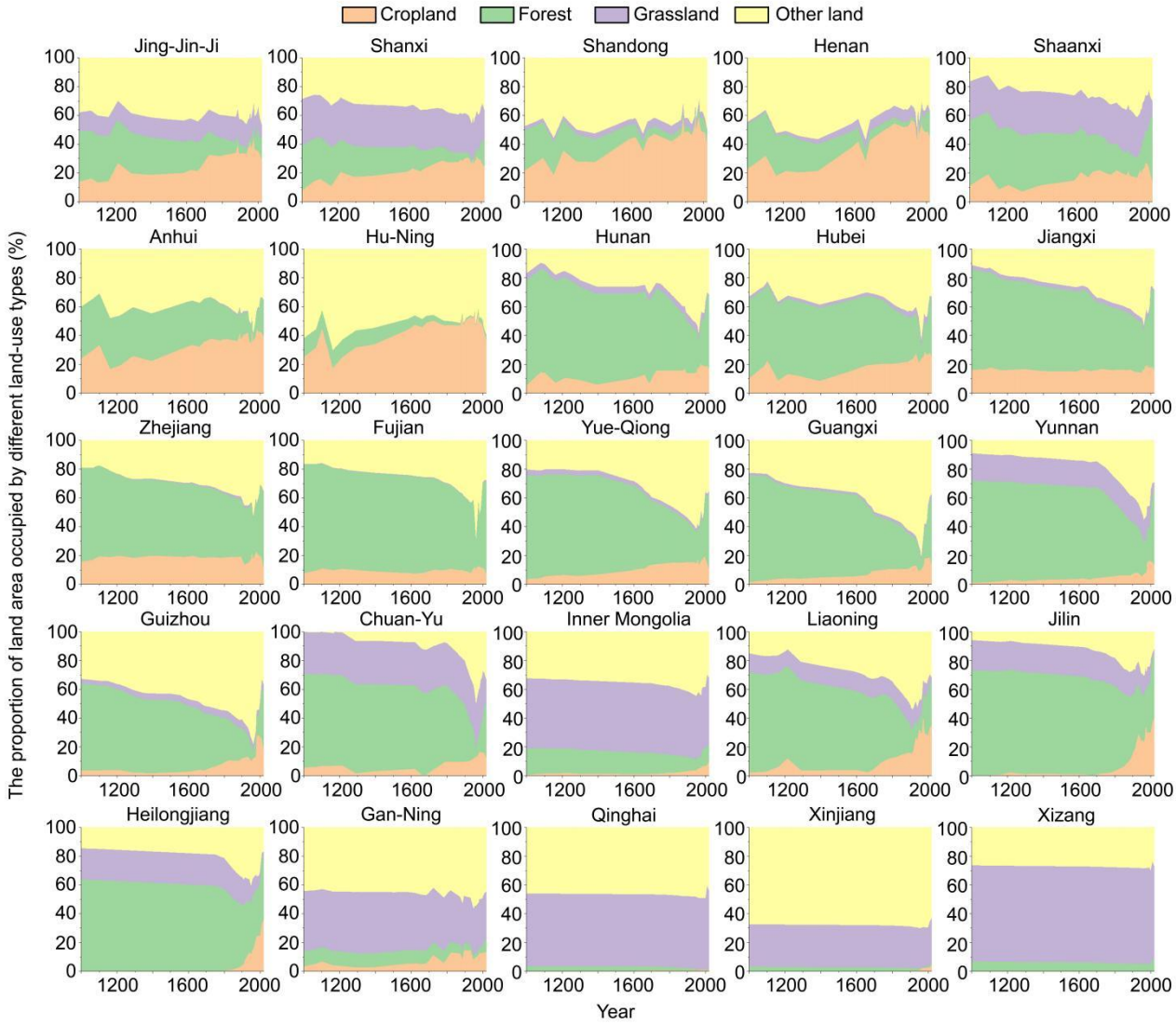


**Figure 3.** Percentage of the area of cropland, forest, grassland, and other land at the provincial scale.

Land-use products derived from remote sensing imagery are spatially explicit, thereby enabling the clear identification of land-use type transitions. However, the provincial-level reconstructed data used in this study lacked explicit spatial location information, and the conversion relationships between different land-use types were not always clear. Therefore, annual land-use conversion rates were difficult to calculate. When only two land-use types are involved and the increase (or decrease) in one land-use type exactly matches the decrease (or increase) in the other type, the conversion between land-use types is relatively straightforward. However, when more than two land-use types are involved in land-use change, the conversion relationships become complex. To address this latter issue, we established rules to prioritize land-use conversions (Fig. 4).

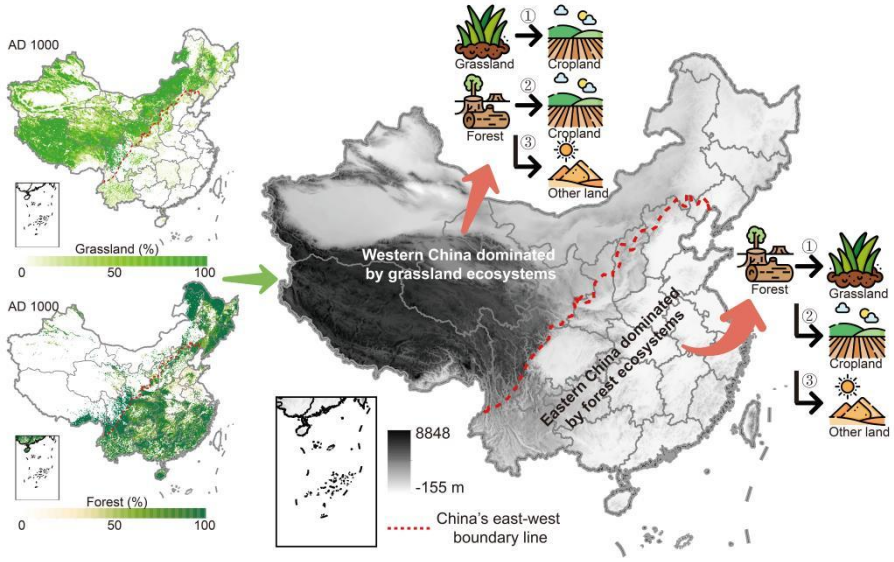


**Figure 4.** Historical land-use change transition rules. Numbers ①, ②, and ③ represent the priority levels.

315

First, the conversion rules were determined based on the attributes of the published data used, which was a prerequisite for establishing the land-use transition rules in this study. The land-use change data revealed the changes in grassland area and their conversion relationships were the most clearly defined. The reconstruction rules for historical grassland data formed the basis of the grassland-related land-use conversion rules in this study. Specifically, when reconstructing historical grassland 320 data in western China, the data reflect the occupation of grassland due to the reclamation of cropland in history (He et al., 2024). Therefore, for western China, where grassland ecosystems dominate, changes in grassland areas primarily reflect the encroachment of croplands, and the conversion between grassland and cropland was determined first based on changes in grassland area (Fig. 4). Second, the reduction in forest area was prioritized for conversion to cropland, followed by conversion to other land. In eastern China, where forest ecosystems are predominant, historical grasslands mainly consisted 325 of secondary grasslands because of the secondary succession of deforested lands (He et al., 2024). Hence, in eastern provinces dominated by forest ecosystems, the conversion between grassland and forest can be similarly determined based on changes in the grassland area. The remaining forest area was then prioritized for conversion to cropland, followed by conversion to other land. Based on these rules, we calculated the annual land-use change rates in China from 1000 to 2019.

Historical conversion of forest to cropland or forest to other land was primarily performed for land reclamation, and if the 330 deforested land supported cultivation over a long period, it was converted to cropland. For cropland that failed to support cultivation due to reasons such as a loss of fertility, it was defined as other land in this study. According to Table B2 in the appendix, in the bookkeeping model used in this study, the disturbance response curves for the conversion of forest to cropland and forest to other land were identical. Therefore, once the land-use conversion rules related to grassland were established, regardless of whether the set priorities or other methods (such as area weighting) were used to handle 335 forest-related land-use conversions, the final carbon emission calculation results were not be affected by the specific

classification of forest conversion into cropland or other land.

Houghton and Castanho (2023) proposed four alternative explanations for forest conversion to other land: Explanation 1: Forest loss is overestimated; Explanation 2: Forests are converted to shifting cultivation; Explanation 3: Forests are converted to new cropland, while an equal area of cropland is abandoned and undergoes degradation; and Explanation 4: Forests are converted to new cropland, while an equal area of cropland is abandoned, and subsequently restored to forest over a long period. Historically, shifting cultivation (through deforestation) was common. Shifting cultivation is a primitive and underdeveloped agricultural practice in which farmers clear land by burning and cultivating it extensively to obtain agricultural products. Once the soil fertility is exhausted, farmers abandon cultivation and continue to clear new land. This practice has been widespread historically and continues today in the tropical rainforest regions of South America, Africa, and Southeast Asia (Heinimann et al., 2017). Based on the characteristics of forest cover change documented in the Chinese historical literature, attributing forest loss to shifting cultivation aligns more closely with historical facts, excluding conversion to cropland and grassland. This form of agriculture has been recorded extensively in Chinese historical documents.

The annual changes in cropland, forest, and grassland areas over the past millennium (Fig. 5a)clearly revealed that between the 18$^{th}$ and mid-20$^{th}$ centuries, the annual loss of forest area greatly exceeded the annual increase in cropland area. Based on the conversion rules assumed here, we derived the annual change in other land (primarily shifting cultivation) over the past millennium (Fig. 5b). The data revealed that shifting cultivation was prevalent throughout history, although its scale was relatively small before the 18$^{th}$ century, with an average annual increase of $6.22\times10^4$ ha. However, after explosive population growth occurred in China, people under the pressure of survival expanded to hilly and mountainous forestlands, and converted large areas of forest via shifting cultivation. The average annual increase in shifting cultivation during this period reached $40.54 \times 10^4$ ha, which was 6.5 times greater than that of the previous period.

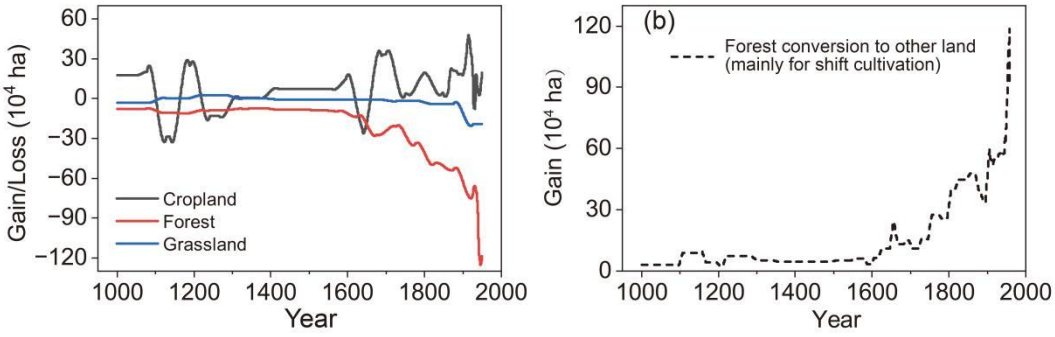


**Figure 5.** Changes in cropland, forest, grassland, and other land areas.

### 2.3.3 Uncertainty assessment

To assess the methodological uncertainty associated with our priority allocation rules, we introduced an area-weighted allocation method for sensitivity analysis. This approach allocates the total area from land use types with a net annual decrease proportionally to those with a net annual increase. We recalculated the annual land use transition matrices for the entire study period using this method and systematically compared them with the results from the priority-based approach. This comparison allowed us to quantify the impact of the allocation rules on the rates of land use change and carbon budget estimations, thereby validating the robustness of our primary findings.

To evaluate the uncertainty in estimating carbon emission fluxes, this study employed Monte Carlo simulations with 1000 iterations. The uncertainty primarily stems from two key parameters: carbon density and land-use change area. For the carbon densities in the forest (aboveground, belowground, and soil) and grassland (aboveground, belowground, and soil) components, the mean and standard deviation were calculated based on input sample data. During the simulations, values for these densities were randomly sampled from normal distributions parameterized based on these statistics measures. Regarding the land-use change area, the original input value for the annual conversion area of each land-use type served as the mean for its sampling distribution, with the standard deviation set to 10% of this mean. Values were then randomly sampled from a normal distribution defined by these parameters in each iteration. Subsequently, in every iteration, the annual carbon emission flux was re-estimated using the parameters sampled in that specific iteration. After aggregating the results from all iterations, the minimum and maximum simulated carbon emission flux values for each year were used to define the uncertainty interval for that year's estimates.

## 3. Results

### 3.1 Overall carbon emissions

The land-use changes and associated carbon emissions in China over the past millennium are illustrated in Fig. 6. From 1000 to 2019, cumulative carbon emissions resulting from land-use changes totaled 19.61 Pg C, with the highest cumulative emissions of 21.87 Pg C occurring around 1980. Overall, due to lag effects, the carbon emission trajectory did not fully align with the timeline of land-use changes. Specifically, the reversal of forest area decline (i.e., the transition from forest loss to forest regrowth) occurred in the 1960s (Fig. 6a and 6b), whereas the reversal of the carbon budget from carbon source to carbon sink occurred in the 1980s. Approximately 30% of the annual carbon emission flux was attributable to residual emissions from historical periods.

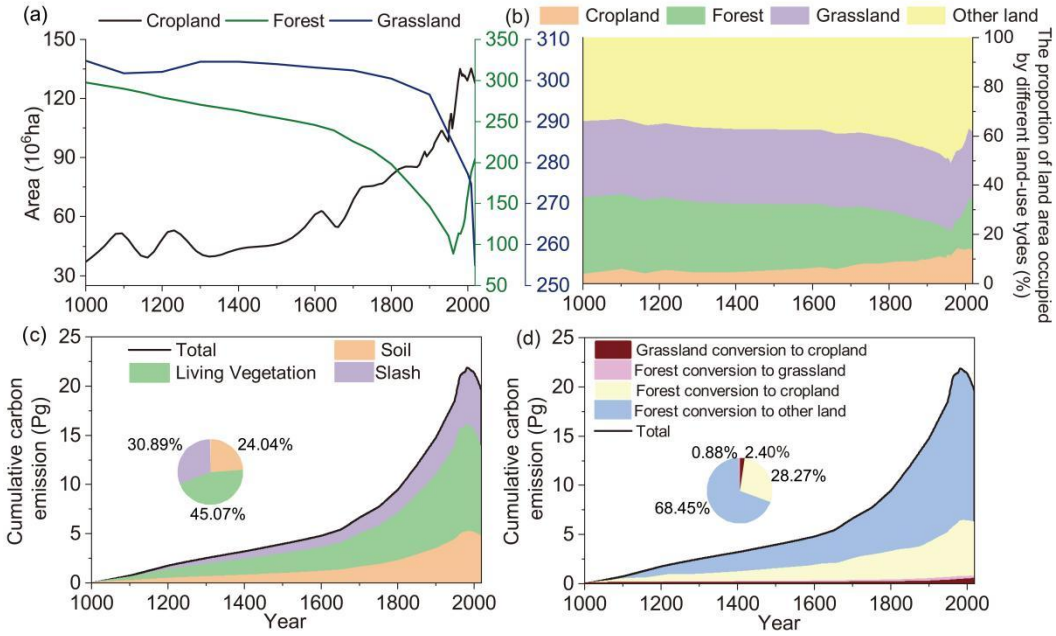


**Figure 6.** Annual land-use changes and carbon emissions in China from 1000 to 2019. (a) Cropland, forest, and grassland areas (absolute values), in units of $10^6$ hectares. (b) Proportions of four land-use types in each period, with all remaining terrestrial cover—excluding the reconstructed cropland, forest, and grassland—classified as other land. (c) Cumulative carbon emissions from land-use changes across different carbon pools. (d) Cumulative carbon emissions from different land-use transitions. In (c) and (d), the two pie charts represent the shares of different carbon pools and land-use transitions in the cumulative carbon emissions over the millennium, respectively.

Based on the clear temporal trajectories, four distinct phases of carbon emissions were identified. Phase 1 (1000–1700): A slow growth phase for carbon sources, driven by deforestation, cropland expansion, and grassland reclamation, which resulted in a cumulative carbon emission of 6.60 Pg C, accounting for 30.17% of the total carbon emissions. The average annual carbon emission in this phase was 9.46 Tg C $yr^{-1}$ (Fig 7a). Phase 2 (1700–1980): A rapid growth phase for carbon sources during which croplands expanded significantly beyond traditional agricultural areas in China, moving to southwest, northeast, and northwest China, accompanied by large-scale deforestation and grassland reclamation. Cumulative carbon emissions during this period reached 15.27 Pg C, accounting for 69.86% of the total emissions. The average annual emission was 54.09 Tg C $yr^{-1}$, 5.7 times that of Phase 1. Phase 3 (1980–1998) was a phase dominated by large-scale afforestation, the carbon budget for land-use changes shifted from being a carbon source to a carbon sink. Between 1980 and 1998, the carbon sink amounted to 0.12 Pg C, with an average annual carbon sink of 16.85 Tg C $yr^{-1}$. Phase 4 (1998–2019): An enhanced carbon sink phase attributed to the widespread implementation of large-scale forestry projects. During this period, the total carbon sink reached 1.85 Pg C (Fig. 6c and 6d), with an average annual carbon sink intensity of 88.21 Tg C $yr^{-1}$ (Fig 7a), which was 5.2 times higher than that of Phase 3.

Regarding carbon pool types, the vegetation carbon pool stood out as the largest contributor to total emissions, accounting for 45.07% of the overall emissions (Fig. 6c). This was reflected in an average annual emission intensity of 8.67 Tg C $yr^{-1}$ (Fig. 7b). Following closely was the slash carbon pool, which contributed 30.89%, with an average annual emission intensity of 5.95 Tg C $yr^{-1}$ (Fig. 7c). The soil carbon pool, while still significant, represented a smaller portion at 24.04%, emitting an

average of 4.63 Tg C $yr^{-1}$ (Fig. 7d). When considering the impact of land-use changes, the conversion of forest to other land types, particularly shifting cultivation, emerged as the most dominant factor. This conversion alone was responsible for a staggering 68.45% of the total carbon emissions (Fig. 6d), with an average annual emission of 13.17 Tg C $yr^{-1}$ (Fig. 7e). The conversion of forest to cropland followed, contributing 28.27% of the emissions, or 5.44 Tg C $yr^{-1}$ (Fig. 7f). In comparison, the conversion of grassland to cropland had a relatively minor effect, accounting for just 2.40% of the emissions, equivalent to 0.46 Tg C $yr^{-1}$ (Fig. 7g). Finally, the conversion of forest to secondary grassland had an almost negligible impact, representing only 0.88% of total emissions, with an annual release of less than 0.01 Tg C $yr^{-1}$.

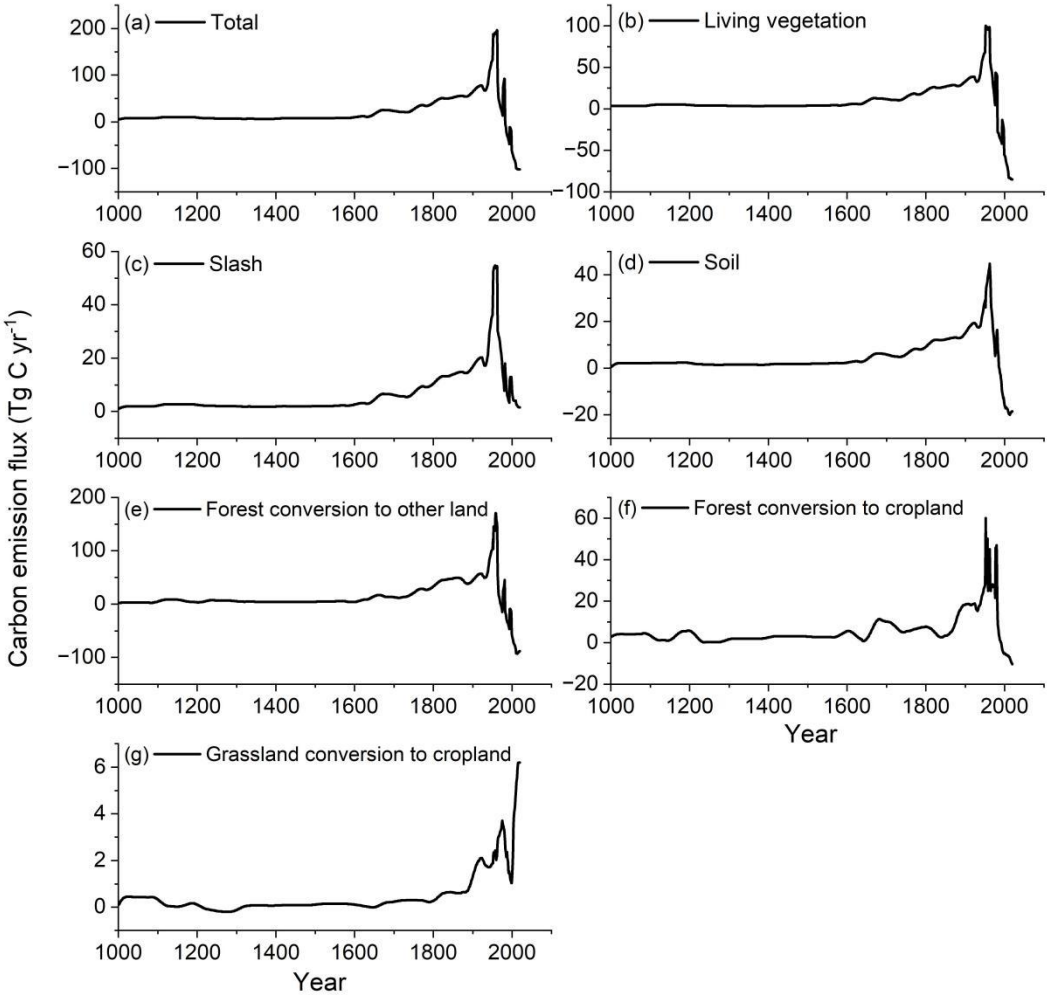


**Figure 7.** Annual carbon emission flux of land-use changes in China from 1000 to 2019: total, carbon pools of soil, vegetation, and slash and different land-use conversions. Annual carbon emission flux from forest conversion to grassland is less than 0.01 Tg C $yr^{-1}$ and thus is not presented in graphical form. Negative values indicate carbon sink fluxes.

### 3.2 Regional carbon emissions

To facilitate the analysis of the spatiotemporal evolution of land-use carbon emissions, this study divided China into five major regions: North China, Southeast China, Southwest China, Northeast China, and Northwest China (Fig. 8). North China

primarily refers to the North China Plain (Beijing, Tianjin, Hebei, Henan, Shandong, Anhui, and Jiangsu) and the provinces Shanxi and Shaanxi. Southeast China includes the provinces Hubei, Hunan, Jiangxi, Zhejiang, Fujian, Guangdong, Hainan, and Guangxi. Southwest China consists of the provinces Sichuan, Chongqing, Guizhou, and Yunnan. Considering the forest coverage in southeastern Xizang, this region is also categorized as part of Southwest China. Northeast China includes the provinces Liaoning, Jilin, and Heilongjiang as well as Inner Mongolia, where forest resources are mainly distributed in the Greater Khingan Range. Northwest China includes the provinces Gansu, Ningxia, Qinghai, and Xinjiang.

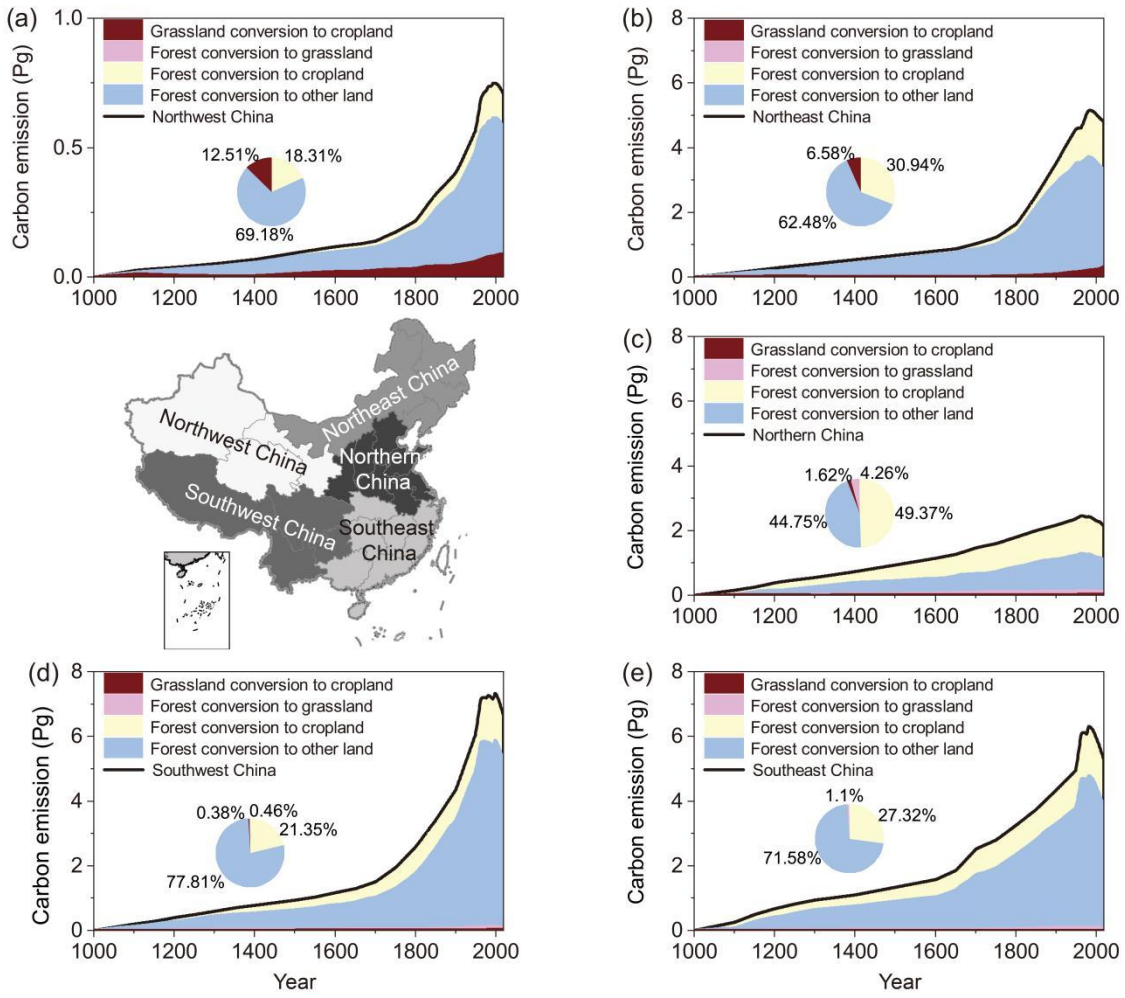


**Figure 8.** Cumulative carbon emissions and their proportions of land-use changes in different regions of China from 1000 to 2019.

Over the past millennium, Southwest China has recorded the highest cumulative carbon emissions, totaling 6.66 Pg C, followed by Southeast China with 5.29 Pg C and Northeast China with 4.81 Pg C. In contrast, North China accounted for 2.15 Pg C, and Northwest China recorded only 0.71 Pg C. Carbon emissions from land-use conversion in these regions showed significant variation. Notably, North China was distinct from the other regions, with the highest proportion of carbon emissions resulting from the conversion of forests to croplands, accounting for 49.37% of the total (Fig. 8c). In the other four regions, the conversion of forests to other land types (mainly shifting cultivation) contributed to the highest proportion of

carbon emissions, with values of 71.58%, 77.81%, 62.48%, and 69.18%. The conversion of forests to secondary grasslands occurred mainly in North China and Southeast China, contributing 4.26% and 1.1% of total carbon emissions, respectively (Fig. 8c and 8e). The conversion of grasslands to cropland occurred mainly in Northwest and Northeast China, accounting for 12.51% and 6.58%, respectively (Fig. 8a and 8b).

At the provincial scale, the years in which land-use changes shifted from carbon sources to carbon sinks varied across regions (Appendix Fig. C1). During the carbon source period, seven provinces had cumulative carbon emissions exceeding 1.00 Pg C or an average carbon emission flux greater than 1.00 Tg C $yr^{-1}$, namely, Chuan-Yu, Yunnan, Heilongjiang, Guangxi, Inner Mongolia, Jilin, and Hunan. Among these, Chuan-Yu had the highest carbon emissions, reaching 3.28 Pg C (with an average carbon emission flux of 3.35 Tg C $yr^{-1}$) (Fig. 9). The cumulative carbon emissions in eight provinces, namely, Guizhou, Yue-Qiong, Liaoning, Hubei, Fujian, Jiangxi, Xizang, and Jing-Jin-Ji, ranged between 0.55 and 0.97 Pg C (average carbon emission flux of 0.58–0.99 Tg C $yr^{-1}$). The remaining 10 provinces had cumulative carbon emissions of less than 0.50 Pg C, with Hu-Ning having the lowest at 0.11 Pg C (0.11 Tg C $yr^{-1}$). During the carbon sink period, the contribution of carbon uptake by each province followed a similar order as the carbon emissions in each province during the carbon source period. The Chuan-Yu region contributed 0.39 Pg C to the carbon sink, with a flux of 10.35 Tg C $yr^{-1}$. This indicates that provinces with significant carbon emissions owing to widespread deforestation and agricultural expansion in historical periods have played an important role as carbon sinks in recent decades, largely through large-scale afforestation and other interventional measures.

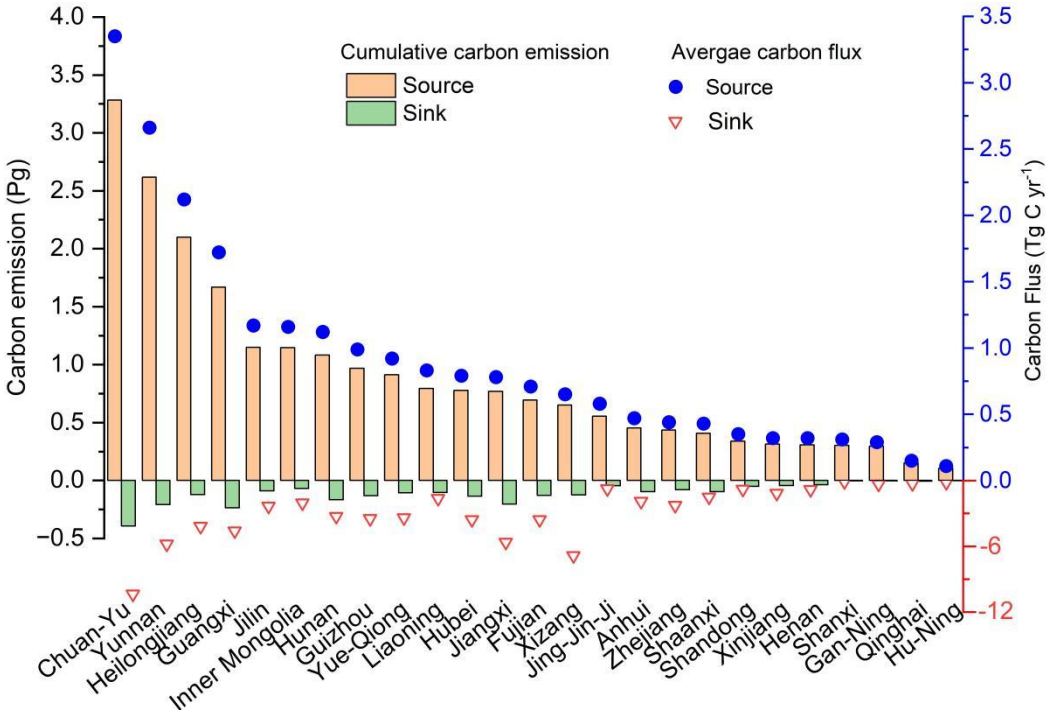


**Figure 9.** Cumulative carbon emissions and average carbon flux at the provincial scale from 1000 to 2019. Jing-Jin-Ji represents the aggregation of Beijing, Tianjin, and Hebei; Hu-Ning represents Shanghai and Jiangsu; Yue-Qiong represents Guangdong and Hainan;

Chuan-Yu represents Sichuan and Chongqing; and Gan-Ning represents Gansu and Ningxia.

### 3.3 Uncertainty and Sensitivity Analysis

To evaluate the impact of the annual land use change calculation rule and to test its robustness, we conducted a systematic sensitivity analysis. We first compared the annual land use transition matrices derived from our priority-based method against those from the area-weighted method. The results show that while numerical differences exist for some transition types (see Appendix Fig. C2), the dominant transition processes, such as forest-to-cropland conversion, demonstrate high consistency, indicating the stability of the primary patterns of land use change identified from the historical data. More crucially, when these two sets of matrices were respectively applied to a carbon bookkeeping model, the resulting national carbon budget time series were highly consistent in their trends and key turning points (Fig. 10). Furthermore, the estimates derived from the area-weighted method fall entirely within the uncertainty bounds of our priority-based results. In summary, this sensitivity analysis provides strong evidence that the choice of calculation rule does not substantively affect the core conclusions of our study on the features and trends of China's millennial-scale land-use change carbon budget, thereby demonstrating the robustness of our methodology.

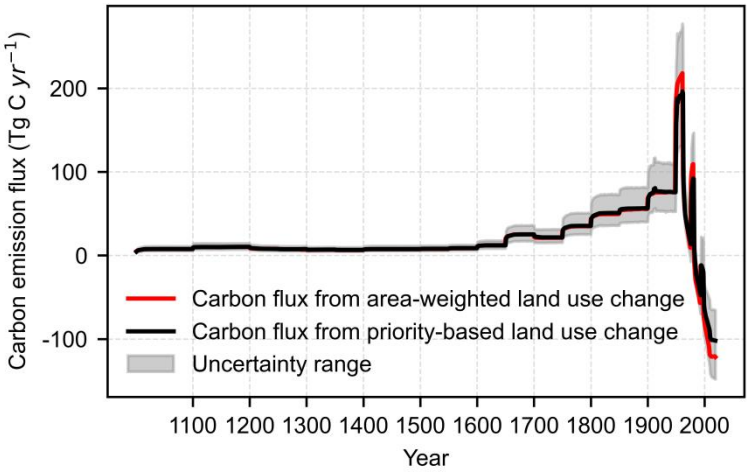


**Figure 10.** Comparison of annual carbon emissions from land-use change using different calculation methods, with uncertainty assessment.

This study employed Monte Carlo simulations (1000 iterations) to systematically assess the uncertainty in annual carbon emission flux estimates (Fig.10). The results revealed that the average annual uncertainty interval, defined as the range between the maximum and minimum simulated emissions, was 18.75 Tg C. This interval exhibited significant interannual variation, ranging from a minimum of 3.77 Tg C to a maximum of 143.67 Tg C. Such variation indicates that the uncertainty in the estimation results correspondingly increased in years characterized by substantial fluctuations in land-use change data. Overall, the Monte Carlo simulations effectively highlighted the impact of parameter uncertainty on carbon emission

estimates and provided a quantitative basis for evaluating the credibility of the carbon flux results. To further constrain parameter variability, future efforts should focus on improving the resolution of measured carbon density data and the reliability of land-use data.

## 4. Discussion

### 4.1 Review of estimation methods

Compared with the carbon emission estimates from land-use changes in China over the past 300 years by Yang et al. (2023), this study updated and improved the land-use change data, carbon density data, and disturbance response curves. The specific improvements were as follows. (1) Building on multiple recent studies, the land-use change data for China from 1700 to 1980 were extended back to AD 1000 and forward to 2019, resulting in a land-use dataset with 131 time points spanning from 1000 to 2019. (2) In the calculation of land-use change rates, Yang et al. (2023) adjusted cropland data to align with 50- and 100-year time intervals, matching those of the forest and grassland data. However, cropland data from historical periods, which were reconstructed based on tax records for cropland areas in historical archives, are highly accurate and record rich information on cropland coverage changes. Adjusting to 50- and 100-year intervals often obscures many signals of cropland cover change, whereas this study preserved all such information. (3) In the process of collecting carbon density data, we incorporated the results from China's Soil Survey Series, specifically the "Soil Series Atlas of China," which compiled 1,253 soil carbon density samples for various land cover types, including forests and grasslands. This significantly enriched the carbon density sample database, making the data more representative. (4) In the calculation of provincial carbon density, we assessed the normal distribution characteristics of the carbon density sample data for each province and chose either the arithmetic mean or median to obtain provincial average carbon densities, minimizing the influence of abnormally high or low values in the samples. (5) Yang et al. (2023) noted that in historical periods, the area of forest converted to cropland was far greater than the area of cropland expansion. However, their study did not clearly explain how this "excess" forest loss was classified. To address this gap, our study classifies the remaining forest change (i.e., deforestation not resulting from cropland occupation) as shifting cultivation. This approach is based on the global historical land-use change scenarios of Houghton and Castanho (2023) and extensive historical records from China, and is more aligned with historical facts. Based on this, we developed land-use conversion rules suitable for provincial-level analysis in China and incorporated the methods and characteristics of cropland, forest, and grassland dataset reconstruction. (6) The disturbance response curve was central to the bookkeeping model, driving the calculation of carbon budgets using annual land-use change rates and carbon density data. In this study, we used the latest published disturbance-response curve (Houghton and Castanho, 2023). In summary, this study updated and improved both the data and models covering six

specific areas, thereby increasing the reliability of carbon emission estimates.

### 4.2 Comparison with previous estimates

The definition of land-use change emissions differs fundamentally between bookkeeping models and Dynamic Global Vegetation Models (DGVMs). Bookkeeping models generally account only for direct human-induced carbon fluxes, whereas DGVMs may also include indirect components such as the "loss of additional sink capacity," leading to systematic differences in estimates. For a comprehensive comparison with prior findings, we adopted two complementary formats structured by data attributes. Table 3 summarizes key studies reporting estimates for specific time periods to allow for a comparison of aggregate amounts. In contrast, Figure 11 assembles studies with accessible annual time-series data to compare their temporal dynamics.

Many scholars have achieved progress in estimating carbon emissions based on long-term land-use changes in China. Among them, Houghton and Castanho (2023), Yang et al. (2023), Yang et al. (2019), Li et al. (2014), and Ge et al. (2008) are particularly comparable to this study because of their long time spans, broad scope, and use of bookkeeping models. While these studies are often considered comparable within the context of the past 300 years, direct comparisons are not entirely accurate due to differing methodologies and data. Using the annual carbon flux estimates in this study, we calculated carbon emissions over periods comparable to those of related studies (Table 3). Specifically, the cumulative carbon emissions from 1700 to 1980 in this study were 68% higher than those estimated by Yang et al. (2023) (Table 3). This difference was primarily due to the significant reduction in forest area, which far exceeds the expansion of cropland in historical periods. This study clearly identified the source of this change as shifting cultivation. The carbon emissions from 1661 to 1980 in this study were 4.28 times higher than those reported by Yang et al. (2019), mainly because the latter only considered the conversion of forest and grassland to cropland. From 1700 to 1949, the carbon emissions in this study were 92% higher than those reported by Ge et al. (2008), which was mainly because of differences in the land-use change rate calculation rules and underlying vegetation and soil carbon density data. At the regional scale, the carbon emissions in this study from 1680 to 1980 in Northeast China (Heilongjiang, Jilin, and Liaoning) were 130% higher than those estimated by Li et al. (2014). Furthermore, this study used an improved bookkeeping model, whereas Yang et al. (2019), Li et al. (2014), Ge et al. (2008), and Yang et al. (2023) all relied on an earlier version, which is another significant source of difference. Overall, the carbon emission estimates in this study were 68% to 328% higher than those of previous studies, indicating that previous estimates of carbon emissions from land-use changes in China may have been severely underestimated.

**Table 3.** Comparison of existing long-term carbon emission estimation results caused by land-use change in China

| Region | Land use type | Method | Time period | Previous study (Pg C) | Reference | This study (Pg C) |
|---|---|---|---|---|---|---|

| | | | | | | |
|---|---|---|---|---|---|---|
| China | Cropland, Forest, Grassland | Bookkeeping model (Early version) | 1700–1980 | 9.05 | Yang et al. (2023) | 15.17 |
| China | Cropland | Bookkeeping model (Early version) | 1661–1980 | 3.78 | Yang et al. (2019) | 16.13 |
| China | Cropland, Forest | Bookkeeping model (Early version) | 1700–1949 | 6.18 | Ge et al. (2008) | 11.87 |
| Northeast China (Heilongjiang, Jilin, and Liaoning) | Cropland | Bookkeeping model (Early version) | 1680–1980 | 1.45 | Li et al. (2014) | 3.33 |
| Global | Cropland, Forest, Grassland, Other land | Bookkeeping model (Latest version) | 1850–2019 | 7.36 | Houghton and Castanho (2023) | 7.72 |
| China | Cropland, Forest | Land ecosystem model | 1900–1980 | 6.90 | Yu et al. (2022) | 7.07 |
| China | Cropland, Forest | Land ecosystem model | 1980–2019 | 8.90 | Yu et al. (2022) | 2.25 |
| China | Cropland, Forest, Grassland, Other land | Bookkeeping model (Latest version) | 1000–2019 | 19.61 | This study | |

Note: Bookkeeping model (Early version) refers to the initial model developed by Houghton and Hackler (2003), while Bookkeeping model (Latest version) refers to the most recently updated model by Houghton and Castanho (2023).

The NGHGI.DB, NGHGI.DB.corrected, and TRENDYv8 datasets used in our study are all adopted from Obermeier et al. (2024). Detailed descriptions of these datasets, including their specific definitions, distinctions, and the correction procedures applied, are provided in Appendix Table D1. Specifically, the TRENDYv8 dataset allows for the isolation of direct LULUCF impacts through the comparison of different scenarios (e.g., with and without land-use change). At the national level, considerable uncertainty is observed among the different methods used to estimate carbon emissions from land-use changes in China. From the carbon emission flux change curve, Our carbon flux estimate is positioned in the mid-range of other models before 2000, while post-2000 it acts as a significant carbon sink, albeit one weaker in magnitude than that recently reported by Zhu et al. (2025). (Fig. 11). Specifically, the cumulative emissions estimated in this study are close to those of Houghton and Nassikas (2017), particularly those of Houghton and Castanho (2023) for China (Table 3), partly because all three rely on the same bookkeeping model. Nevertheless, significant differences were observed in the carbon flux peaks and valleys among the three studies (Fig. 11), mainly because of substantial differences in the provincial-level land-use data. A recent study by Zhu et al. (2025) reports a more pronounced trend, with higher carbon emissions in 1981–1991 and a much larger carbon sink in 1992–2020 (Fig. 11), likely due to their use of remote-sensing products combined with national forest inventory data, which may better capture deforestation and afforestation dynamics.

The estimates from the other three bookkeeping models aligned more closely with the trends in the DGVM estimates, which were markedly different from our estimations. This discrepancy primarily stems from two key aspects. First, DGVM estimates often account for the “loss of additional sink capacity”. This concept refers to the diminished carbon absorption

that occurs when the land-use type of a parcel of land that could have absorbed more carbon dioxide under current environmental conditions if left in its original natural state (e.g., as a forest) is altered by human activities (e.g., conversion to cropland), thereby reducing its actual carbon dioxide uptake. This "reduction in absorbed amount" constitutes the loss of additional sink capacity. Gasser et al. (2020) revealed that the inclusion or exclusion of loss of additional sink capacity leads to significant differences in estimated values. Second, disparities in land-use change forcing data represent another significant factor contributing to divergent estimates among different models. DGVM estimates are typically driven by long-term global land-use datasets, such as LUH2 (Obermeier et al., 2024; Friedlingstein et al., 2025; Hansis et al., 2015). Thus, these models that differ due to the inclusion of loss of additional sink capacity and the use of varying land-use change data tend to significantly overestimate the carbon emission flux from land-use changes relative to the results of this study.

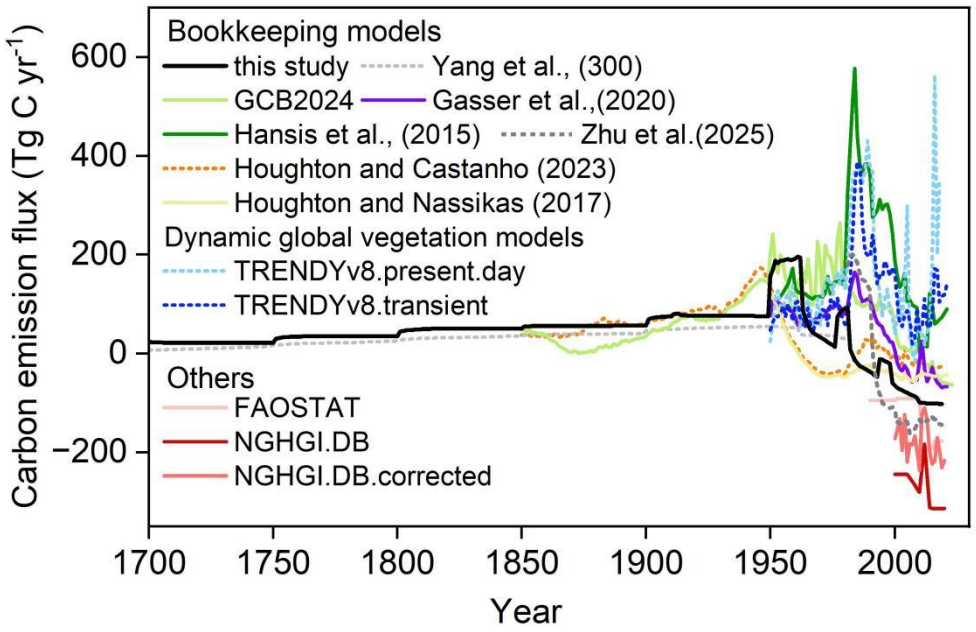


**Figure 11.** Chinese historical land-use change-induced carbon emission flux estimated by different methods. The GCB estimate synthesizes the findings of Gasser (2020), Hansis et al. (2015), and Houghton (2023).

Additionally, the estimates from this study differed considerably from national report-based data (e.g., NGHGIs and FAOSTAT) (Fig. 11) (Obermeier et al., 2024). The core difference between NGHGIs and bookkeeping models in land-use change carbon flux estimation lies in the carbon accounting boundary, especially regarding the attribution of indirect fluxes on managed land (Gidden et al., 2023; He et al., 2024). NGHGIs tend to consider all carbon fluxes on managed land (including both direct fluxes and indirect fluxes triggered by environmental changes) as anthropogenic contributions. In contrast, bookkeeping models primarily account for direct fluxes generated by direct human activities but exclude indirect fluxes, which are considered natural ecosystem responses, from anthropogenic inventories of land-use change. The fact that national reports specifically account for afforestation and ecological restoration projects with high carbon removal potential might also influence the results. The most direct example is the similarity between our estimated carbon emissions

(1900–1980) and the results of Yu et al. (2022) (Table 3) because of the lack of significant or widespread land management or engineering projects in China during this period. However, the estimates for 1980–2019 differed greatly because land management practices during this period had a substantial impact. As revealed by Yue et al. (2024), land management has played a crucial role in China's land-carbon balance since 1980.

### 4.3 Implications and Applications

For regional carbon budget assessment, the dataset provides a robust historical baseline for carbon fluxes from land-use change, enabling the separation of legacy emissions from contemporary fluxes. This is crucial for accurately attributing the drivers of the current terrestrial carbon sink and evaluating the effectiveness of ecological restoration efforts. In climate and Earth system modeling, the dataset serves as an independent benchmark for evaluating and refining DGVMs. Validation against the provincially-resolved emission estimates from this study can help constrain model parameters related to ecosystem responses to land-use change. For policy evaluation, the dataset offers long-term quantitative evidence to assess the efficacy of land-use policies. The key transition from a carbon source to a sink around the 1980s strongly coincides with the implementation of China's large-scale ecological restoration policies, thus supporting the assessment of the potential effectiveness of such national-level interventions.

### 4.4 Limitations

This study utilizes data from the Second and Third National Land Surveys to link with reconstructed historical data. Compared to annual remote sensing-based land use products, the national survey data is more compatible with the reconstructed historical data in terms of its sources and inherent characteristics. However, we acknowledge that discrepancies exist in the classification standards and statistical calibers across different periods, such as the changes between the Second and Third surveys. To mitigate the impact of these inconsistencies, we made a specific adjustment for the forest land category, a key factor in the carbon cycle. According to the definition in the source literature for the reconstructed historical data, its conceptualization of 'forest' most closely aligns with 'closed forest land' in the current classification standards. Therefore, we used the 'closed forest land' sub-category, under the primary 'forest land' category from the Second and Third surveys, to ensure definitional consistency. Despite this effort, we recognize that the differences in statistical calibers among data sources remain a source of uncertainty in our carbon budget estimation, which awaits future improvement through more refined data harmonization and calibration methods. The long-term land-use data used in this study, including reconstructed and derived data from statistical surveys, represent the net land-use values within the statistical units. However, actual land-use changes, as indicated by remote sensing data, show that within a given area of a

particular land-use type, certain pixels represent either increased area or decreased area. The total change due to these increases and decreases is much greater than the net change, and such detailed variations cannot currently be captured by long-term historical land-use datasets. Therefore, uncertainty in basic land-use data leads to inherent uncertainty in the estimated carbon budget associated with land-use changes.

When calculating annual land-use change rates, the classification of land-use types is relatively coarse due to data limitations. Land-use types other than cropland, forest, and grassland are all grouped together as "other land," and land-use conversion rules are established based on this classification to calculate the annual land-use change rates. Compared with modern remote sensing-based land-use data, long-term land-use data are less detailed, which also affects the accuracy of carbon budget estimates related to land-use change.

Additionally, the spatiotemporal variability of basic carbon density values can influence the accuracy of the estimates. In this study, carbon density is addressed using a "present-day-for-past" substitution method. Although modern soil carbon densities were moderately adjusted by incorporating a large-scale soil sampling survey dataset from the post-1949 period in China, pre-industrial carbon stocks likely varied due to shifts in atmospheric $CO_2$ concentrations, climate fluctuations, ecological succession, and human land management. Vegetation and soil carbon densities were not static over the past millennium. Therefore, using static values to represent historical carbon densities may fail to capture temporal dynamics, thereby introducing uncertainties. Potential biases include overestimating human contributions if climate-driven increases in carbon density are ignored and overestimating modern carbon uptake if long-term baseline declines in carbon stocks are not included. Future studies should explore coupling DGVMs (e.g., LPJ or ORCHIDEE) to simulate combined impacts of historical climate, $CO_2$ levels, and human activities on carbon density. In this study, to quantitatively assess the uncertainty introduced by the assumption of static carbon density, we conducted a sensitivity analysis. This analysis was based on two core hypotheses: 1) historical vegetation carbon density was 20% lower than modern values, accounting for the reduced $CO_2$ fertilization effect in the pre-industrial era; and 2) historical soil carbon density was 20% higher, reflecting less intensive anthropogenic disturbance and more intact ecosystems. The results show that this scenario leads to a systematic reduction in the estimated annual net carbon emissions and reveals distinct temporal patterns. During the dominant carbon source periods, this reduction was relatively stable (mean annual difference of approx. -2 Tg C $yr^{-1}$). In contrast, during carbon sink periods, which were often accompanied by intense land-use change, the discrepancy between the two estimates exhibited greater volatility, leading to a significant amplification of uncertainty in these phases. This trend indicates that using static modern carbon density values may lead to an overestimation of the historical carbon source effect.

We reiterate that the carbon emission accounting method in the present study does not include wood harvesting. Considering that wood harvesting represents a significant historical source of anthropogenic emissions, the absence of these data may lead to a certain degree of underestimation in the corresponding carbon emission fluxes. Fortunately, Houghton and Castanho (2023) estimated China's long-term carbon emissions from wood harvesting and found values of 5 Tg C $yr^{-1}$ for

2011–2020, approximately 20–30 Tg C $yr^{-1}$ around the 1950s, approximately 5–10 Tg C $yr^{-1}$ in the 1900s, and less than 5 Tg C $yr^{-1}$ values before 1900. These estimates can serve as a reference when regional long-term reconstructed data on wood harvesting and their corresponding carbon emission estimates are unavailable.

## 5. Data availability

The dataset of annual carbon emissions from land-use change in China (1000–2019) is available at https://doi.org/10.5281/zenodo.14557386 (Yang et al., 2025).

## 6. Conclusion

Reducing the uncertainty in carbon budget estimates from land-use change has become a frontier in global change science and is receiving widespread attention, as it plays a crucial role in achieving the global "carbon neutrality" target. This study provides an estimation of the annual carbon emissions from land-use changes in China from 1000 to 2019. High-confidence long-term land-use change datasets, extensive vegetation and soil carbon density sampling data, and the latest published disturbance-response curves effectively minimized the uncertainties in previous long-term carbon budget estimates for China.

From 1000 to 2019, carbon emissions resulting from land-use changes in China amounted to 19.61 Pg C. Four distinct phases were identified. The first phase, which occurred before the early 18th century (1000–1700), saw a slow increase in carbon sources, with a total emission of 6.60 Pg C, accounting for 30.17% of the total, at an average annual rate of 9.46 Tg C $yr^{-1}$. The second phase, which occurred from the early 18th century to the early 1980s (1700–1980), experienced rapid growth in carbon sources (15.27 Pg C, 69.86%, 54.09 Tg C $yr^{-1}$). The third phase, which occurred from the 1980s to the late 1990s (1980–1998), saw a reversal in the carbon balance, with land-use changes shifting from carbon sources to carbon sinks (carbon sink of 0.12 Pg C, 16.85 Tg C $yr^{-1}$). The fourth phase, which occurred from the late 1990s to 2019 (1998–2019), saw a further enhancement of the carbon sink (1.85 Pg C, 88.21 Tg C $yr^{-1}$).

**Author contributions.** FY and GD designed the work. FY, FH, and ML provided historical provincial cropland, forest, and grassland data for quantifying China's annual carbon budget from land-use change. FY, WL, ZL, and XZ collected vegetation and soil carbon density sample point data. RAH provided the disturbance-response curve parameter table. FY, XM, RAH, and YG devised the land-use transition rules. FY, GD, XM, HZ, PW, FH, QM, YY, BL and CY reviewed and edited the text. FY prepared the manuscript and drafted the manuscript with contributions from all coauthors.

**Competing interests.** One of the (co-)authors is a member of the editorial board of Earth System Science Data.

**Disclaimer.** Publisher's note: Copernicus Publications remains neutral with regard to jurisdictional claims made in the text, published maps, institutional affiliations, or any other geographical representation in this paper. While Copernicus Publications makes every effort to include appropriate place names, the final responsibility lies with the authors. Publisher's remark: please note that Figs. 1, 4, 8, and B1 contain disputed territories.

**Financial support.** This research has been supported by the National Key Research and Development Program of China (No. 2023YFB3907403, 2017YFA0603304), the National Natural Science Foundation of China (No. 42201263), and the Key Scientific and Technological Project of Henan Province (No. 232102321103).

## Appendix A

**Table A1.** Detailed reference for the second and third national land survey bulletins.

| Items | Time point | Land-use types | Province | Data source/Download link |
|---|---|---|---|---|
| The Second National Land Survey of China | 2009 | cropland, forest, and grassland | all provinces | https://gtdc.mnr.gov.cn/shareportal#/ |
| | | | Henan | https://www.henan.gov.cn/2022/04-18/2433857.html |
| | | | Shanxi | http://www.shanxi.gov.cn/ywdt/zwlb/bmkx/202201/t20220127_6441197.shtml |
| | | | Shandong | http://dnr.shandong.gov.cn/zwgk_324/xxgkml/ywdt/tzgg_29303/202112/t20211216_3810111.html |
| | | | Hebei | https://zrzy.hebei.gov.cn/heb/gongk/gkml/gggs/qtgg/zrdcc/10671417206794772480.html |
| | | | Liaoning | https://www.ln.gov.cn/web/ywdt/jrln/wzxx2018/EFA7CA9476D44D8D85578D867D70EA56/index.shtml |
| | | | Jilin | http://www.jl.gov.cn/szfzt/xwfb/xwfbh/xwfbh2021/jlsdssjrmdbdhdychy_409635/ |
| | | | Heilongjiang | http://www.dview.com.cn/rjcp_zz_3741.html |
| | | | Jiangsu | http://news.yznews.com.cn/2021-12/31/content_7347606.htm |
| | | | Zhejiang | https://zrzyt.zj.gov.cn/art/2021/12/3/art_1289933_58988406.html |
| | | | Anhui | https://zrzyt.ah.gov.cn/public/7021/146407571.html |
| The Third National Land Survey of China | 2019 | cropland, forest, and grassland | Fujian | http://zrzyt.fujian.gov.cn/zwgk/zfxxgkzl/zfxxgkml/tdgl_19753/202112/t20211231_5805488.htm |
| | | | Jiangxi | http://bnr.jiangxi.gov.cn/art/2021/12/29/art_35804_3810534.html |
| | | | Hubei | https://zrzyt.hubei.gov.cn/fbjd/xxgkml/sjfb/tdzytjsj/202112/t20211217_3919353.shtml?eqid=e3b66db3004cc51a00000006647fe835 |
| | | | Hunan | http://www.hunan.gov.cn/hnszf/zfsj/sjfb/202112/t20211207_21275973.html?share_token=83aa6011-7231-4c49-8a14-a14f9ae0c29b |
| | | | Guangdong | http://www.jiangmen.gov.cn/jmzrj/gkmlpt/content/2/2507/post_2507058.html?eqid=87430417001fc53900000003648a53ca#187 |
| | | | Hainan | https://www.hainan.gov.cn/hainan/0101/202110/8c92db59ef6f4468b96b058465ba60b2.shtml |
| | | | Sichuan | http://dnr.sc.gov.cn/scdnr/scsdcsj/2022/1/18/3e1bc5eb55db44628498b5db740eac5b.shtml |
| | | | Guizhou | http://www.guizhou.gov.cn/zwgk/zdlygk/jjgzlfz/zrzy/zrzydcjcgl/202201/t20220121_72378280.html |
| | | | Yunnan | https://www.yn.gov.cn/sjfb/tjgb/202112/t20211221_231929.html |

| | | |
|---|---|---|
| | Shaanxi | https://zrzyt.shaanxi.gov.cn/info/1038/57862.htm?eqid=892a22b000028c4b00000006644b72c5 |
| | Gansu | https://baijiahao.baidu.com/s?id=1712097491056856575&wfr=spider&for=pc |
| | Qinghai | https://zrzyt.qinghai.gov.cn/gk/sj/zrzygb/content_4922 |
| | Beijing | https://ghzrzyw.beijing.gov.cn/zhengwuxinxi/sjtj/tdbgdctj/202111/t20211105_2529986.html |
| | Tianjin | https://ghhzrzy.tj.gov.cn/zwgk_143/tzgg/202111/t20211118_5712899.html |
| | Shanghai | https://ghzyj.sh.gov.cn/zcfg-tdgl/20220107/b513d306e88b41bebc7b7b8a5b5cc56c.html |
| | Chongqing | http://tjj.cq.gov.cn/zwgk_233/fdzdgknr/tjxx/sjzl_55471/tjgb_55472/202111/t20211125_10031239.html |
| | Inner Mongolia | https://zrzy.nmg.gov.cn/zwgk/tztg/202205/t20220507_2051673.html |
| | Guangxi | https://dnr.gxzf.gov.cn/zfxxgk/fdzdgknr/tjfx/zhtj/t16084757.shtml |
| | Xizang | http://zrzyt.xizang.gov.cn/gk/gsgg/202112/t20211224_276279.html |
| | Ningxia | https://www.nx.gov.cn/zwgk/tzgg/202112/t20211206_3205422_zzb.html |
| | Xinjiang | http://zrzyt.xinjiang.gov.cn/xjgtzy/gzdt/202201/c7061f858692402da4f7b65e376cd2fb.shtml |

* Last access: May 2024.

## Appendix B

**Table B1.** Detailed information for soil series in China

| Title | Publisher | Year |
|---|---|---|
| Soil Series in China: Anhui | Science Press | 2017 |
| Soil Series in China: Beijing and Tianjin | Science Press | 2016 |
| Soil Series in China: Hebei | Science Press | 2017 |
| Soil Series in China: Shandong | Science Press | 2019 |
| Soil Series in China: Henan | Science Press | 2019 |
| Soil Series in China: Jiangsu | Science Press | 2017 |
| Soil Series in China: Shanghai | Science Press | 2017 |
| Soil Series in China: Hubei | Science Press | 2017 |
| Soil Series in China: Fujian | Science Press | 2017 |
| Soil Series in China: Zhejiang | Science Press | 2017 |
| Soil Series in China: Hainan | Science Press | 2018 |
| Soil Series in China: Heilongjiang | Science Press | 2020 |
| Soil Series in China: Jilin | Science Press | 2019 |
| Soil Series in China: Liaoning | Science Press | 2020 |
| Soil Series in China: Guangdong | Science Press | 2017 |
| Soil Series in China: Central and Western Volume: Shanxi | Science Press<br>Longmen Press | 2020 |
| Soil Series in China: Central and Western Volume: Shaanxi | Science Press<br>Longmen Press | 2020 |
| Soil Series in China: Central and Western Volume: Inner Mongolia | Science Press<br>Longmen Press | 2020 |
| Soil Series in China: Central and Western Volume: Ningxia | Science Press<br>Longmen Press | 2020 |
| Soil Series in China: Central and Western Volume: Qinghai | Science Press<br>Longmen Press | 2020 |
| Soil Series in China: Central and Western Volume: Hunan | Science Press<br>Longmen Press | 2020 |
| Soil Series in China: Central and Western Volume: Jiangxi | Science Press<br>Longmen Press | 2020 |
| Soil Series in China: Central and Western Volume: Sichuan | Science Press<br>Longmen Press | 2020 |
| Soil Series in China: Central and Western Volume: Chongqing | Science Press<br>Longmen Press | 2020 |
| Soil Series in China: Central and Western Volume: Gansu | Science Press<br>Longmen Press | 2020 |
| Soil Series in China: Central and Western Volume: Guangxi | Science Press<br>Longmen Press | 2020 |
| Soil Series in China: Central and Western Volume: Guizhou | Science Press<br>Longmen Press | 2020 |
| Soil Series in China: Central and Western Volume: Yunnan | Science Press<br>Longmen Press | 2020 |
| Soil Series in China: Central and Western Volume: Xinjiang | Science Press<br>Longmen Press | 2020 |

**Table B2.** Disturbance response curve parameter.

| Ecological zone | Land-use change | Soil decay | Soil recovery |
|---|---|---|---|
| Temperate Desert | FC, FO, GC | 3% per year (first 4 years)<br>1% per year (last 11 years ) | 0.3% per year (50 years) |
| Temperate Steppe | FC, FO, GC | 3% per year (first 4 years)<br>1% per year (last 11 years ) | 0.41% per year (37 years) |
| Temperate Continental | FC, FO, GC | 3% per year (first 4 years)<br>1% per year (last 11 years ) | 0.3125% per year (48 years) |
| Subtropical Humid | FC, FO, GC | 3% per year (first 4 years)<br>1% per year (last 11 years ) | 0.3125% per year (48 years) |
| **Ecological zone** | **Land-use change** | **Living vegetation decay** | **Living vegetation recovery** |
| Temperate Desert | FC, FO | 95% per year (1 year) | 0.02% per year (50 years)<br>0.06% per year (30 years) |
| | FG | 95% per year (1 year) | 0.05% per year (28 years)<br>0.09% per year (20 years) |
| Temperate Steppe | FC, FO | 95% per year (1 year) | 0.24% per year (37 years)<br>0.09% per year (50 years) |
| | FG | 90% per year (1 year) | 0.11% per year (37 years)<br>0.09% per year (50 years) |
| Temperate Continental | FC, FO | 95% per year (1 year) | 1.63% per year (48 years)<br>0.56% per year (50 years) |
| | FG | 90% per year (1 year) | 1.99% per year (37 years)<br>0.56% per year (50 years) |
| Subtropical Humid | FC, FO | 95% per year (1 year) | 1.63% per year (48 years)<br>0.56% per year (50 years) |
| | FG | 90% per year (1 year) | 1.99% per year (37years)<br>0.56% per year (50 years) |
| **Ecological zone** | **Land-use change** | **Fraction Goes to Slash** | **Decay rate** |
| Temperate Desert, Temperate Steppe, Temperate Continental | FC, FO | 50% | 10% each year based on the value of the previous year |
| | FG | 33% | |
| Subtropical Humid | FC, FO | 50% | 50% each year based on the value of the previous year |
| | FG | 33% | |

Note: FC refers to the conversion between Forest and Cropland. FO refers to the conversion between Forest and Other land. FG refers to the conversion between Forest and Grassland. GC refers to the conversion between Grassland and Cropland.

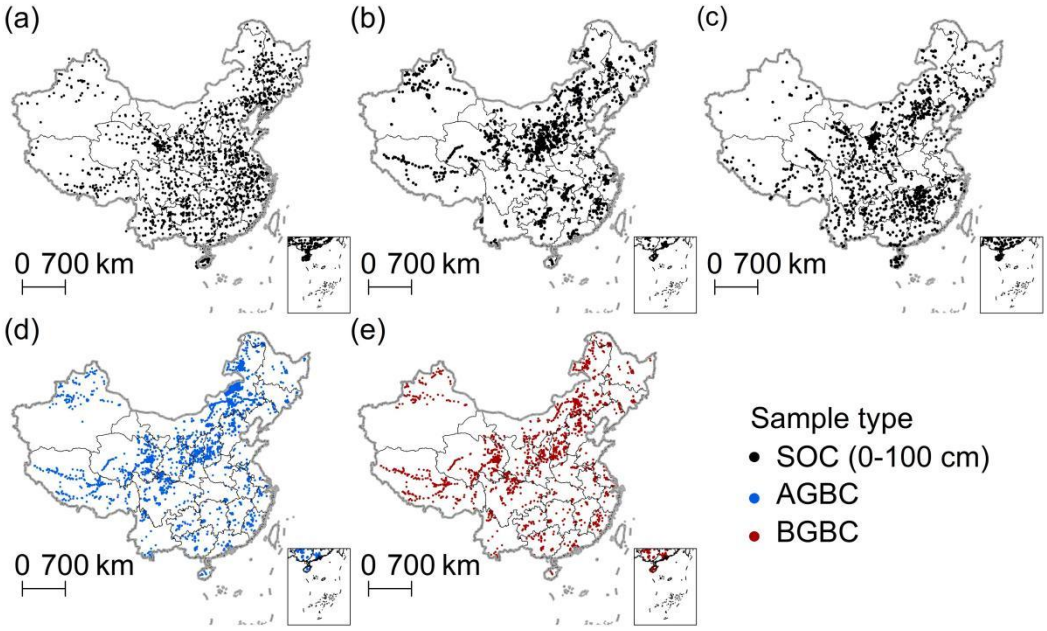


**Figure B1.** Distribution of sample points for vegetation carbon density and soil carbon density. (a) SOC is derived from the 2010s China's terrestrial ecosystem carbon density dataset (Xu et al., 2019). (b) SOC is derived from the "Soil Chronicles of China." (c) SOC is derived from the "Soil Series of China." SOC refers to soil organic carbon. AGBC refers to above-ground biomass carbon, and BGBC refers to below-ground biomass carbon.

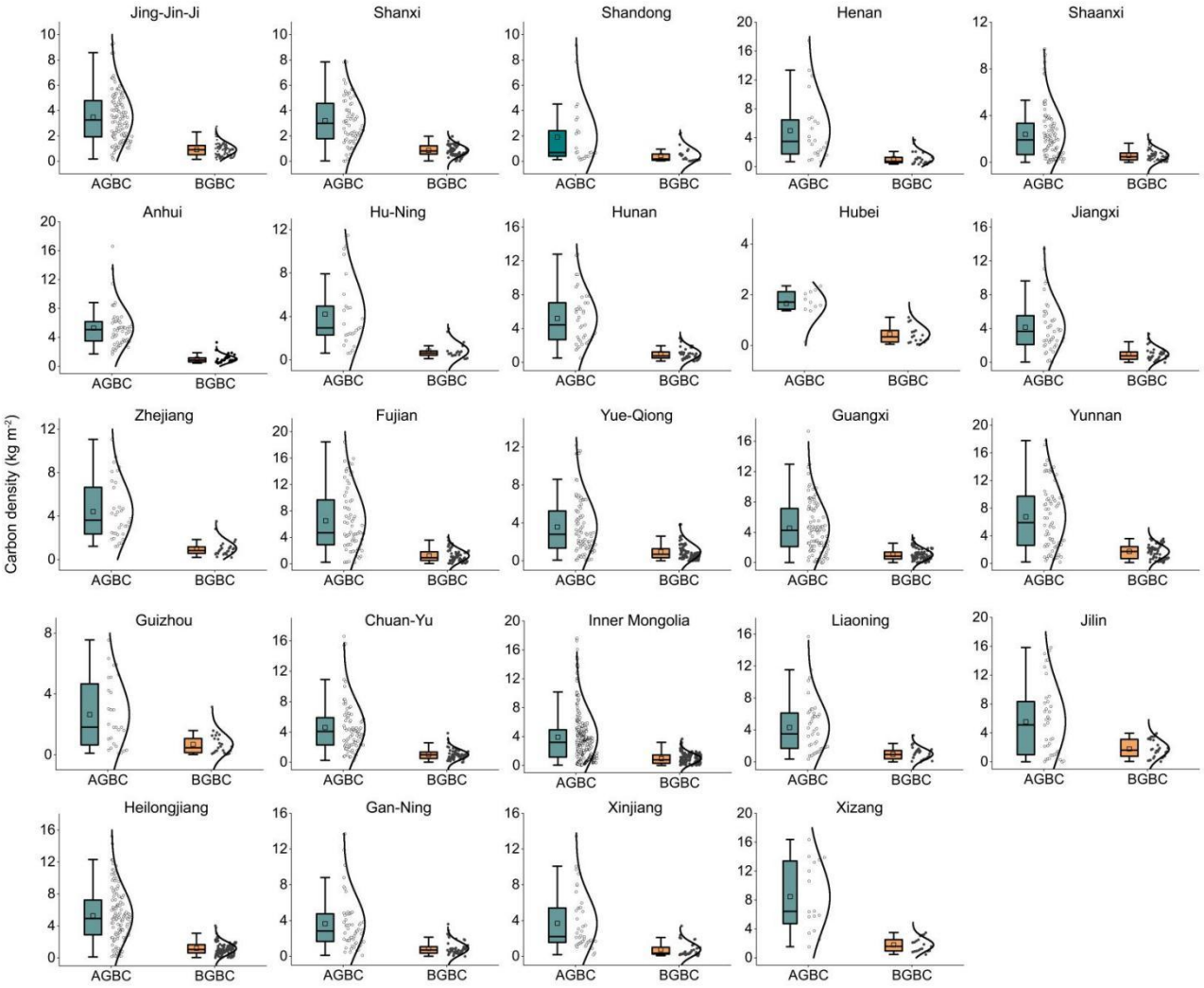


**Figure B2.** Distribution of forest vegetation carbon density at provincial scale. AGBC refers to above-ground biomass carbon, and BGBC refers to below-ground biomass carbon.

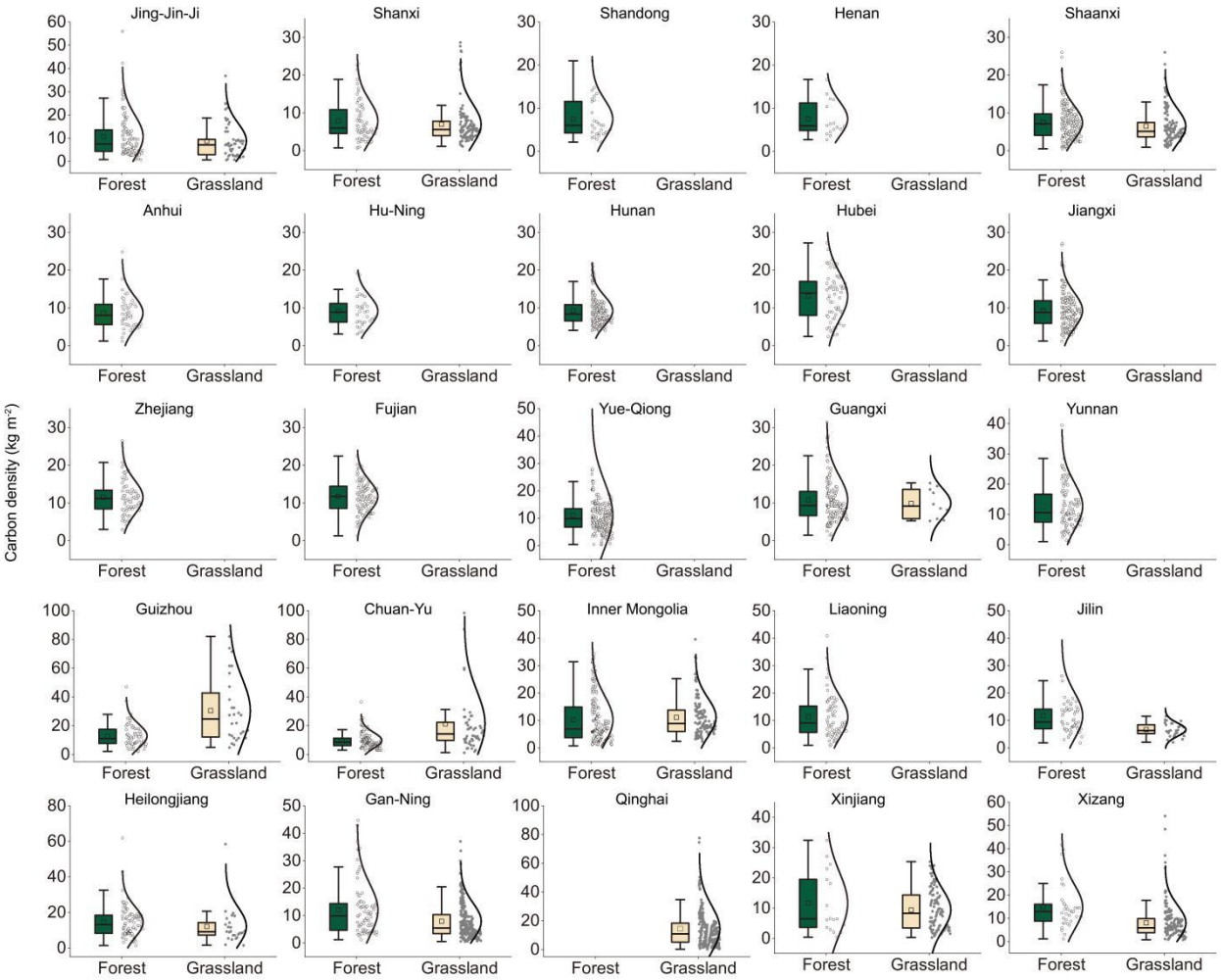


**Figure B3.** Distribution of soil carbon density in forests and grasslands at provincial scale.

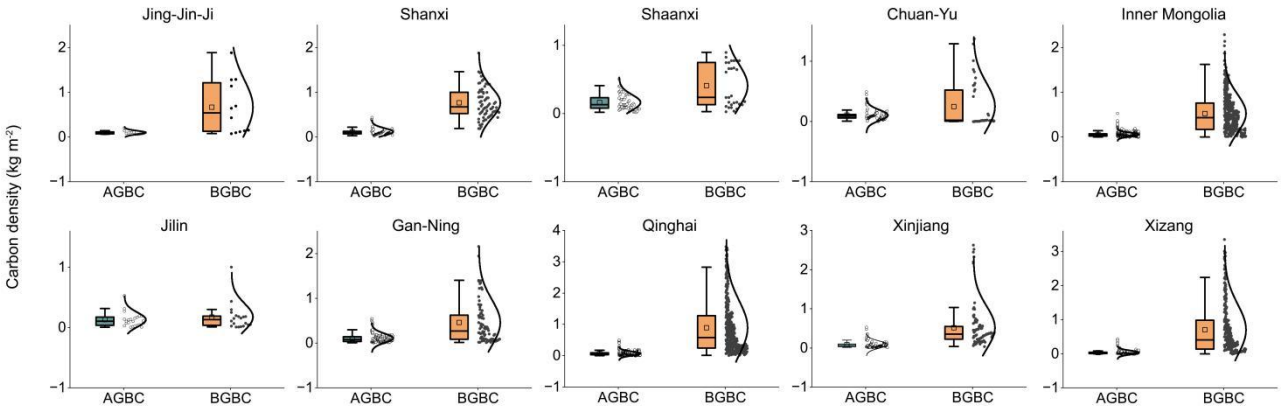


**Figure B4.** Distribution of grassland vegetation carbon density at provincial scale. AGBC refers to above-ground biomass carbon, and BGBC refers to below-ground biomass carbon.

## Appendix C

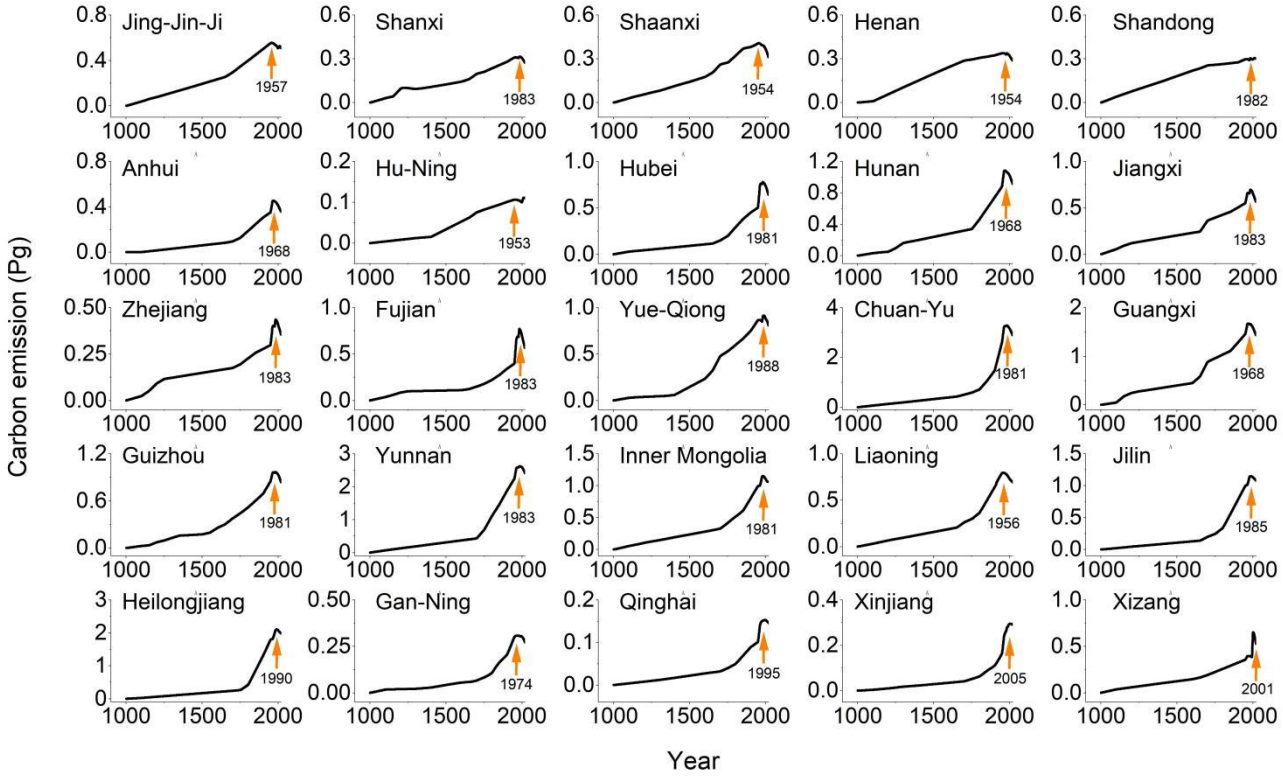


**Figure C1.** Cumulative carbon emissions from land-use changes at the provincial level. Arrows indicate the turning points from carbon sources to carbon sinks, with numbers representing the corresponding years of the turning points.

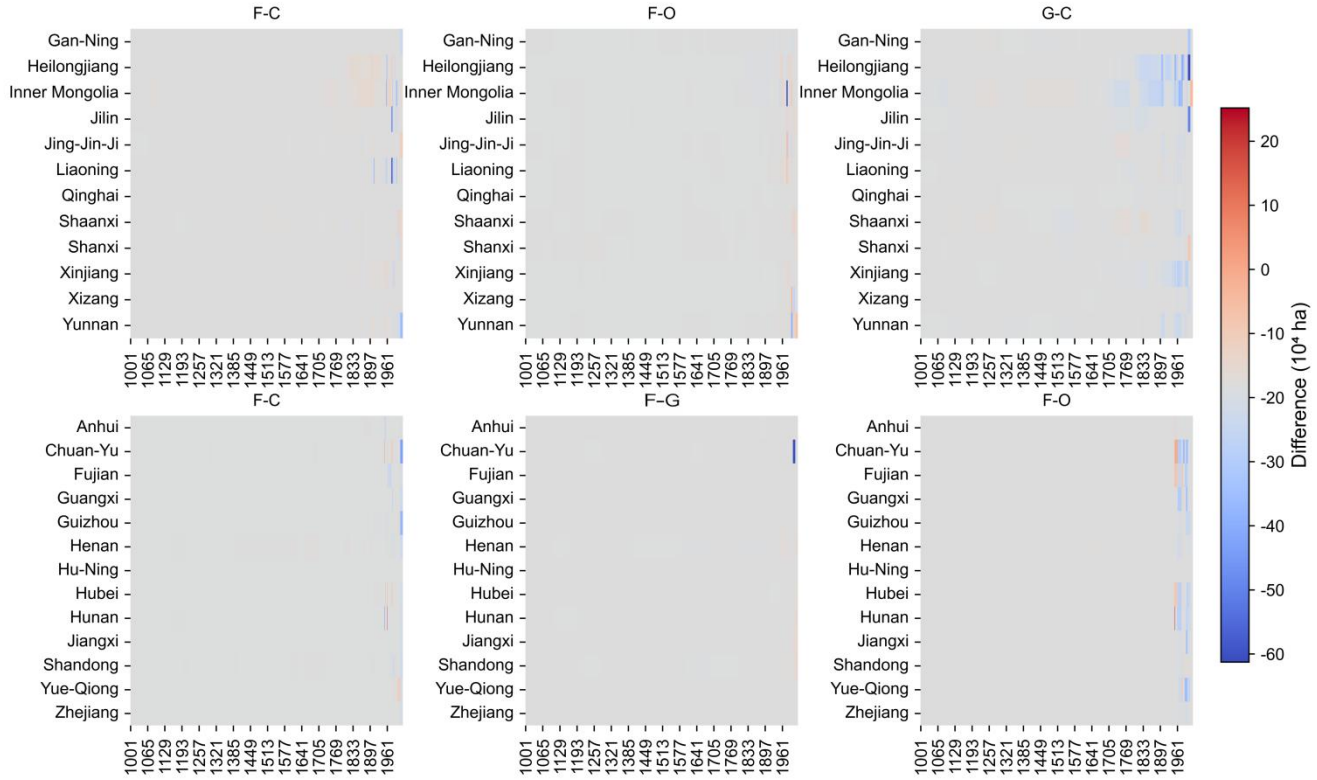


**Figure C2**. Differences in annual land-use transitions between the priority-based and area-weighted allocation methods. F-C denotes the conversion between Forest and Cropland, F-G represents Forest-Grassland conversion, F-O represents Forest-Other land conversion, and G-C represents Grassland-Cropland conversion. A positive difference indicates that the priority-based result is lower than the area-weighted result, and vice versa.

## Appendix D

**Table D1.** Definitions and methodologies for the NGHGI.DB, NGHGI.DB.corrected, and TRENDYv8 datasets.

| Dataset | Source and Description | Core Processing and Application |
|---|---|---|
| NGHGI.DB | National Greenhouse Gas Inventory (NGHGI) data reported by countries to the UNFCCC, with gap-filling applied. | Serves as the baseline data representing officially reported carbon fluxes from managed land. |
| NGHGI.DB.corrected | A corrected version of NGHGI.DB, adjusted to align with model-estimated anthropogenic fluxes. | Carbon fluxes from natural and indirect effects (e.g., $CO_2$ fertilization, climate change) are subtracted. This component is estimated by TRENDYv11 models under a scenario without land-use change. |
| TRENDYv8 | Ensemble mean of nine Dynamic Global Vegetation Models (DGVMs). | Used to isolate the direct impacts of LULUCF by comparing results from different scenarios (e.g., with and without land-use change). |

### References


Bastos, A., Hartung, K., Nutzel, T. B., Nabel, J., Houghton, R. A., and Pongratz, J.: Comparison of uncertainties in land-use change fluxes from bookkeeping model parameterisation, Earth System Dynamics, 12, 745-762, 10.5194/esd-12-745-2021, 2021.

Chen, Y., Syvitski, J.P., Gao, S., Overeem, I. and Kettner, A.J.: Socio-economic impacts on flooding: a 4000-year history of the Yellow River, China. Ambio, 41(7): 682-98, 2012.

Dorgeist, L., Schwingshackl, C., Bultan, S., and Pongratz, J.: A consistent budgeting of terrestrial carbon fluxes, Nat Commun, 15, 7426, 10.1038/s41467-024-51126-x, 2024.

Fang, X. Q., Zhao, W. Y., Zhang, C. P., Zhang. D. Y., Wei, X. Q., Qiu W, Ye Y.: Methodology for credibility assessment of historical global LUCC datasets, Science China Earth Sciences, 63: 1013-1025, 10.1007/s11430-019-9555-3, 2020.

FAO: FAOSTAT Statistical Database, FAO, Rome, Extracted from: http://www.fao.org/faostat/en/#data/ (last access: October 2023), 2021.

Friedlingstein, P., Jones, M. W., O'Sullivan, M., Andrew, R. M., Bakker, D. C. E., Hauck, J., Le Quéré, C., Peters, G. P., Peters, W., Pongratz, J., Sitch, S., Canadell, J. G., Ciais, P., Jackson, R. B., Alin, S. R., Anthoni, P., Bates, N. R., Becker, M., Bellouin, N., Bopp, L., Chau, T. T. T., Chevallier, F., Chini, L. P., Cronin, M., Currie, K. I., Decharme, B., Djeutchouang, L. M., Dou, X., Evans, W., Feely, R. A., Feng, L., Gasser, T., Gilfillan, D., Gkritzalis, T., Grassi, G., Gregor, L., Gruber, N., Gürses, Ö., Harris, I., Houghton, R. A., Hurtt, G. C., Iida, Y., Ilyina, T., Luijkx, I. T., Jain, A., Jones, S. D., Kato, E., Kennedy, D., Klein Goldewijk, K., Knauer, J., Korsbakken, J. I., Körtzinger, A., Landschützer, P., Lauvset, S. K., Lefèvre, N., Lienert, S., Liu, J., Marland, G., McGuire, P. C., Melton, J. R., Munro, D. R., Nabel, J. E. M. S., Nakaoka, S.-I., Niwa, Y., Ono, T., Pierrot, D., Poulter, B., Rehder, G., Resplandy, L., Robertson, E., Rödenbeck, C., Rosan, T. M., Schwinger, J., Schwingshackl, C., Séférian, R., Sutton, A. J., Sweeney, C., Tanhua, T., Tans, P. P., Tian, H., Tilbrook, B., Tubiello, F., van der Werf, G. R., Vuichard, N., Wada, C., Wanninkhof, R., Watson, A. J., Willis, D., Wiltshire, A. J., Yuan, W., Yue, C., Yue, X., Zaehle, S., and Zeng, J.: Global Carbon Budget 2021, Earth System Science Data, 14, 1917-2005, 10.5194/essd-14-1917-2022, 2022.

Friedlingstein, P., O'Sullivan, M., Jones, M. W., Andrew, R. M., Bakker, D. C. E., Hauck, J., Landschützer, P., Le Quéré, C., Luijkx, I. T., Peters, G. P., Peters, W., Pongratz, J., Schwingshackl, C., Sitch, S., Canadell, J. G., Ciais, P., Jackson, R. B., Alin, S. R., Anthoni, P., Barbero, L., Bates, N. R., Becker, M., Bellouin, N., Decharme, B., Bopp, L., Brasika, I. B. M.,

Cadule, P., Chamberlain, M. A., Chandra, N., Chau, T.-T.-T., Chevallier, F., Chini, L. P., Cronin, M., Dou, X., Enyo, K., Evans, W., Falk, S., Feely, R. A., Feng, L., Ford, D. J., Gasser, T., Ghattas, J., Gkritzalis, T., Grassi, G., Gregor, L., Gruber, N., Gürses, Ö., Harris, I., Hefner, M., Heinke, J., Houghton, R. A., Hurtt, G. C., Iida, Y., Ilyina, T., Jacobson, A. R., Jain, A., Jarníková, T., Jersild, A., Jiang, F., Jin, Z., Joos, F., Kato, E., Keeling, R. F., Kennedy, D., Klein Goldewijk, K., Knauer, J., Korsbakken, J. I., Körtzinger, A., Lan, X., Lefèvre, N., Li, H., Liu, J., Liu, Z., Ma, L., Marland, G., Mayot, N., McGuire, P. C., McKinley, G. A., Meyer, G., Morgan, E. J., Munro, D. R., Nakaoka, S.-I., Niwa, Y., O'Brien, K. M., Olsen, A., Omar, A. M., Ono, T., Paulsen, M., Pierrot, D., Pocock, K., Poulter, B., Powis, C. M., Rehder, G., Resplandy, L., Robertson, E., Rödenbeck, C., Rosan, T. M., Schwinger, J., Séférian, R., Smallman, T. L., Smith, S. M., Sospedra-Alfonso, R., Sun, Q., Sutton, A. J., Sweeney, C., Takao, S., Tans, P. P., Tian, H., Tilbrook, B., Tsujino, H., Tubiello, F., van der Werf, G. R., van Ooijen, E., Wanninkhof, R., Watanabe, M., Wimart-Rousseau, C., Yang, D., Yang, X., Yuan, W., Yue, X., Zaehle, S., Zeng, J., and Zheng, B.: Global Carbon Budget 2023, Earth System Science Data, 15, 5301-5369, 10.5194/essd-15-5301-2023, 2023.

Friedlingstein, P., O'Sullivan, M., Jones, M. W., Andrew, R. M., Hauck, J., Olsen, A., Peters, G. P., Peters, W., Pongratz, J., Sitch, S., Le Quéré, C., Canadell, J. G., Ciais, P., Jackson, R. B., Alin, S., Aragão, L. E. O. C., Arneth, A., Arora, V., Bates, N. R., Becker, M., Benoit-Cattin, A., Bittig, H. C., Bopp, L., Bultan, S., Chandra, N., Chevallier, F., Chini, L. P., Evans, W., Florentie, L., Forster, P. M., Gasser, T., Gehlen, M., Gilfillan, D., Gkritzalis, T., Gregor, L., Gruber, N., Harris, I., Hartung, K., Haverd, V., Houghton, R. A., Ilyina, T., Jain, A. K., Joetzjer, E., Kadono, K., Kato, E., Kitidis, V., Korsbakken, J. I., Landschützer, P., Lefèvre, N., Lenton, A., Lienert, S., Liu, Z., Lombardozzi, D., Marland, G., Metzl, N., Munro, D. R., Nabel, J. E. M. S., Nakaoka, S.-I., Niwa, Y., O'Brien, K., Ono, T., Palmer, P. I., Pierrot, D., Poulter, B., Resplandy, L., Robertson, E., Rödenbeck, C., Schwinger, J., Séférian, R., Skjelvan, I., Smith, A. J. P., Sutton, A. J., Tanhua, T., Tans, P. P., Tian, H., Tilbrook, B., van der Werf, G., Vuichard, N., Walker, A. P., Wanninkhof, R., Watson, A. J., Willis, D., Wiltshire, A. J., Yuan, W., Yue, X., and Zaehle, S.: Global Carbon Budget 2020, Earth System Science Data, 12, 3269-3340, 10.5194/essd-12-3269-2020, 2020.

Friedlingstein, P., O'Sullivan, M., Jones, M. W., Andrew, R. M., Hauck, J., Landschützer, P., Le Quéré, C., Li, H., Luijkx, I. T., Olsen, A., Peters, G. P., Peters, W., Pongratz, J., Schwingshackl, C., Sitch, S., Canadell, J. G., Ciais, P., Jackson, R. B., Alin, S. R., Arneth, A., Arora, V., Bates, N. R., Becker, M., Bellouin, N., Berghoff, C. F., Bittig, H. C., Bopp, L., Cadule, P., Campbell, K., Chamberlain, M. A., Chandra, N., Chevallier, F., Chini, L. P., Colligan, T., Decayeux, J., Djeutchouang, L. M., Dou, X., Duran Rojas, C., Enyo, K., Evans, W., Fay, A. R., Feely, R. A., Ford, D. J., Foster, A., Gasser, T., Gehlen, M., Gkritzalis, T., Grassi, G., Gregor, L., Gruber, N., Gürses, Ö., Harris, I., Hefner, M., Heinke, J., Hurtt, G. C., Iida, Y., Ilyina, T., Jacobson, A. R., Jain, A. K., Jarníková, T., Jersild, A., Jiang, F., Jin, Z., Kato, E., Keeling, R. F., Klein Goldewijk, K., Knauer, J., Korsbakken, J. I., Lan, X., Lauvset, S. K., Lefèvre, N., Liu, Z., Liu, J., Ma, L., Maksyutov, S., Marland, G., Mayot, N., McGuire, P. C., Metzl, N., Monacci, N. M., Morgan, E. J., Nakaoka, S.-I., Neill, C., Niwa, Y., Nützel, T., Olivier, L., Ono, T., Palmer, P. I., Pierrot, D., Qin, Z., Resplandy, L., Roobaert, A., Rosan, T. M., Rödenbeck, C., Schwinger, J., Smallman, T. L., Smith, S. M., Sospedra-Alfonso, R., Steinhoff, T., Sun, Q., Sutton, A. J., Séférian, R., Takao, S., Tatebe, H., Tian, H., Tilbrook, B., Torres, O., Tourigny, E., Tsujino, H., Tubiello, F., van der Werf, G., Wanninkhof, R., Wang, X., Yang, D., Yang, X., Yu, Z., Yuan, W., Yue, X., Zaehle, S., Zeng, N., and Zeng, J.: Global Carbon Budget 2024, Earth Syst. Sci. Data, 17, 965–1039, https://doi.org/10.5194/essd-17-965-2025, 2025.

Gasser, T., Crepin, L., Quilcaille, Y., Houghton, R.A., Ciais, P. and Obersteiner, M.: Historical $CO_2$ emissions from land use and land cover change and their uncertainty. Biogeosciences, 17(15): 4075-4101, 2020.

Gidden, M.J., Gasser, T., Grassi, G., Forsell, N., Janssens, I., Lamb, W.F., Minx, J., Nicholls, Z., Steinhauser, J. and Riahi, K.: Aligning climate scenarios to emissions inventories shifts global benchmarks. Nature, 624(7990): 102-108, 2023.

Ge, Q. S., Dai, J. H., He, F. N., Pan, Y., and Wang, M. M.: Land use changes and their relations with carbon cycles over the past 300 a in China, Science China: Earth Sciences, 51, 871-884, 10.1007/s11430-008-0046-z, 2008.

Ge, Q. S., Dai, J. H., He, F. N., Zheng, J. Y., Man, Z. M., and Zhao, Y.: Spatiotemporal dynamics of reclamation and cultivation and its driving factors in parts of China during the last three centuries, Progress in Natural Science, 14, 605-613, 2004.

Hansis, E., Davis, S. J., and Pongratz, J.: Relevance of methodological choices for accounting of land use change carbon

fluxes, Global Biogeochemical Cycles, 29, 1230-1246, 10.1002/2014gb004997, 2015.

Hartung, K., Bastos, A., Chini, L., Ganzenmüller, R., Havermann, F., Hurtt, G. C., Loughran, T., Nabel, J. E. M. S., Nützel, T., Obermeier, W. A., and Pongratz, J.: Bookkeeping estimates of the net land-use change flux-a sensitivity study with the CMIP6 land-use dataset, Earth System Dynamics, 12, 763-782, 10.5194/esd-12-763-2021, 2021.

He, F. N., Ge, Q. S., Dai, J. H., and Rao, Y. J.: Forest change of China in recent 300 years, Journal of Geographical Sciences, 18, 59-72, 10.1007/s11442-008-0059-8, 2008.

He, F., Li, S. C., Yang, F., and Li, M. J.: Evaluating the accuracy of Chinese pasture data in global historical land use datasets, Science China Earth Sciences, 61, 1685-1696, 10.1007/s11430-018-9256-1, 2018.

He, F., Li, S., and Zhang, X.: A spatially explicit reconstruction of forest cover in China over 1700-2000, Global and Planetary Change, 131, 73-81, 10.1016/j.gloplacha.2015.05.008, 2015.

He, F., Yang, F., and Wang, Y.: Reconstructing forest and grassland cover changes in China over the past millennium, Science China Earth Sciences, 67, 10.1007/s11430-024-1454-4, 2024.

He, F., Yang, F., Zhao, C., Li, S., and Li, M.: Spatially explicit reconstruction of cropland cover for China over the past millennium, Science China Earth Sciences, 66, 111-128, 10.1007/s11430-021-9988-5, 2023.

He, Y., Piao, S., Ciais, P., Xu, H. and Gasser, T.: Future land carbon removals in China consistent with national inventory. Nature Communications, 15(1): 10426, 2024.

Heinimann, A., Mertz, O., Frolking, S., Egelund Christensen, A., Hurni, K., Sedano, F., Parsons Chini, L., Sahajpal, R., Hansen, M., and Hurtt, G.: A global view of shifting cultivation: Recent, current, and future extent, Plos One, 12, e0184479, 10.1371/journal.pone.0184479, 2017.

Houghton, R. A. and Castanho, A.: Annual emissions of carbon from land use, land-use change, and forestry from 1850 to 2020, Earth System Science Data, 15, 2025-2054, 10.5194/essd-15-2025-2023, 2023.

Houghton, R. A. and Hackler, J. L.: Sources and sinks of carbon from land-use change in China, Global Biogeochemical Cycles, 17, 1034, 10.1029/2002GB001970, 2003, 2003.

Houghton, R. A. and Nassikas, A. A.: Global and regional fluxes of carbon from land use and land cover change 1850–2015, Global Biogeochemical Cycles, 31, 456-472, 10.1002/2016gb005546, 2017.

Houghton, R. A., House, J. I., Pongratz, J., van der Werf, G. R., DeFries, R. S., Hansen, M. C., Le Quéré, C., and Ramankutty, N.: Carbon emissions from land use and land-cover change, Biogeosciences, 9, 5125-5142, 10.5194/bg-9-5125-2012, 2012.

Hurtt, G. C., Chini, L., Sahajpal, R., Frolking, S., Bodirsky, B. L., Calvin, K., Doelman, J. C., Fisk, J., Fujimori, S., Klein Goldewijk, K., Hasegawa, T., Havlik, P., Heinimann, A., Humpenöder, F., Jungclaus, J., Kaplan, J. O., Kennedy, J., Krisztin, T., Lawrence, D., Lawrence, P., Ma, L., Mertz, O., Pongratz, J., Popp, A., Poulter, B., Riahi, K., Shevliakova, E., Stehfest, E., Thornton, P., Tubiello, F. N., van Vuuren, D. P., and Zhang, X.: Harmonization of global land use change and management for the period 850–2100 (LUH2) for CMIP6, Geoscientific Model Development, 13, 5425-5464, 10.5194/gmd-13-5425-2020, 2020.

Jia, R., Fang, X., and Ye, Y.: Gridded reconstruction of cropland cover changes in Northeast China from AD 1000 to 1200, Regional Environmental Change, 23, 10.1007/s10113-023-02118-y, 2023.

Kabora, T. K., Stump, D., Thomas, C. D., and Beale, C. M.: Assessing inconsistencies in historical land-use reconstructions for Africa at 1800, Regional Environmental Change, 24, 10.1007/s10113-024-02224-5, 2024.

Kaplan, J. O., Ruddiman, W. F., Crucifix, M. C., Oldfield, F. A., Krumhardt, K. M., Ellis, E. C., Ruddiman, W. F., Lemmen, C., and Klein Goldewijk, K.: Holocene carbon emissions as a result of anthropogenic land cover change, The Holocene, 21, 775-791, 10.1177/0959683610386983, 2011.

Klein Goldewijk, K., Beusen, A., Doelman, J., and Stehfest, E.: Anthropogenic land use estimates for the Holocene - HYDE 3.2, Earth System Science Data, 9, 927-953, 10.5194/essd-9-927-2017, 2017.

Klein Goldewijk, K.: Estimating global land use change over the past 300 years: The HYDE Database, Global Biogeochemical Cycles, 15, 417-433, 10.1029/1999GB001232, 2001.

Li, B. B., Fang, X. Q., Y, Y., and Zhang, X. Z.: Carbon emissions induced by cropland expansion in Northeast China during the past 300 years, Science China: Earth Sciences, 57, 2259-2268, 2014.

Li, M. J., He, F. N., Li, S. C., and Yang, F.: Reconstruction of the cropland cover changes in eastern China between the 10(th) century and 13(th) century using historical documents, Scientific Reports, 8, 13552, 10.1038/s41598-018-31807-6, 2018a.

Li, M. J., He, F. N., Yang, F., and Li, S. C.: Reconstructing provincial cropland area in eastern China during the early Yuan Dynasty(AD1271-1294), Journal of Geographical Sciences, 28, 1994-2006, 10.1007/s11442-018-1576-8, 2018b.

Li, M., He, F., Yang, F., and Zhao, L.: Reconstruction of provincial cropland area and its spatial-temporal characteristics in the Ming Dynasty, Geographical research, 39, 447-460, 10.11821/dlyj020181315, 2020.

Li, S. C., He, F. N., and Zhang, X. Z.: A spatially explicit reconstruction of cropland cover in China from 1661 to 1996, Regional Environmental Change, 16, 417-428, 10.1007/s10113-014-0751-4, 2016.

Mendelsohn, R. and Sohngen, B.: The net carbon emissions from historic land use and land use change, Journal of Forest Economics, 34, 263-283, 10.1561/112.00000505, 2019.

Obermeier, W. A., Schwingshackl, C., Bastos, A., Conchedda, G., Gasser, T., Grassi, G., Houghton, R. A., Tubiello, F. N., Sitch, S., and Pongratz, J.: Country-level estimates of gross and net carbon fluxes from land use, land-use change and forestry, Earth System Science Data, 16, 605-645, 10.5194/essd-16-605-2024, 2024.

Pongratz, J., Reick, C. H., Raddatz, T., and Claussen, M.: Effects of anthropogenic land cover change on the carbon cycle of the last millennium, Global Biogeochemical Cycles, 23, GB4001, 10.1029/2009gb003488, 2009.

Pongratz, J., Reick, C., Raddatz, T., and Claussen, M.: A reconstruction of global agricultural areas and land cover for the last millennium, Global Biogeochemical Cycles, 22, GB3018, 10.1029/2007gb003153, 2008.

Qin, Z., Zhu, Y., Canadell, J. G., Chen, M., Li, T., Mishra, U., and Yuan, W.: Global spatially explicit carbon emissions from land-use change over the past six decades (1961–2020), One Earth, 7, 1-13, 10.1016/j.oneear.2024.04.002, 2024.

Ramankutty, N. and Foley, J. A.: Estimating historical changes in global land cover: Croplands from 1700 to 1992, Global Biogeochemical Cycles, 13, 997-1027, 10.1029/1999GB900046, 1999.

Soil Species of China. Volume 1-6. Beijing: China Agriculture Press, 1995.

Tan, Q. X.: The Historical Atlas of China: The Sixth Book. Beijing: SinoMaps Press, 1982.

Wedderburn-Bisshop, G.: Deforestation—a call for consistent carbon accounting, Environmental Research Letters, 19, 111006, 10.1088/1748-9326/ad7d21, 2024.

Wei, X., Ye, Y., Li, B., and Chen, T.: Reconstructing cropland change since 1650 AD in Shaanxi province, central China, Quaternary International, 641, 74-86, 10.1016/j.quaint.2022.02.025, 2022.

Winkler, K., Yang, H., Ganzenmüller, R., Fuchs, R., Ceccherini, G., Duveiller, G., Grassi, G., Pongratz, J., Bastos, A., Shvidenko, A., Araza, A., Herold, M., Wigneron, J.-P., and Ciais, P.: Changes in land use and management led to a decline in Eastern Europe's terrestrial carbon sink, Communications Earth & Environment, 4, 237, 10.1038/s43247-023-00893-4, 2023.

Wu, X., Wei, Y., Fu, B., Wang, S. and Moran, E.F.: Evolution and effects of the social-ecological system over a millennium in China's Loess Plateau. Science Advances, 6(41): eabc0276, 2020.

Xu, L., He, N., and Yu, G.: A dataset of carbon density in Chinese terrestrial ecosystems (2010s), China Sci. Data 4, 49-54, 2019.

Yang, F., Dong, G., Meng, X., Gao, Y., He, F., Li, M., Li, W., Liu, Z., Zhai, X., Wu, P., Zhang, H., Mao, Q., Yao, Y., and Yue, C.: Annual carbon emissions from land use change in China from 1000 to 2019 [Data set]. Zenodo. https://doi.org/10.5281/zenodo.14557386, 2025.

Yang, F., He, F. N., Li, M. J., and Li, S. C.: Evaluating the reliability of global historical land use scenarios for forest data in China, Journal of Geographical Sciences, 30, 1083-1094, 10.1007/s11442-020-1771-2, 2020.

Yang, F., He, F., Li, S., Li, M., and Wu, P.: A new estimation of carbon emissions from land use and land cover change in China over the past 300 years, Science of The Total Environment, 863, 160963, 10.1016/j.scitotenv.2022.160963, 2023.

Yang, X., Jin, X., Xiang, X., Fan, Y., Liu, J., Shan, W., and Zhou, Y.: Carbon emissions induced by farmland expansion in China during the past 300 years, Science China Earth Sciences, 62, 423–437, 10.1007/s11430-017-9221-7, 2019.

Yang, X., Jin, X., Xue, Q., and Zhou, Y.: Reconstruction of the spatial distribution of historical farmland in the Taiwan Province of China for 1659-1945, Land Use Policy, 114, 105951, 10.1016/j.landusepol.2021.105951, 2022.

Yang, Y., Mohammat, A., Feng, J., Zhou, R., Fang, J.: Storage, patterns and environmental controls of soil organic carbon in China, Biogeochemistry, 84, 131-141, 2007.

Ye, Y., Fang, X. Q., Ren, Y. Y., Zhang, X. Z., and Chen, L.: Cropland cover change in Northeast China during the past 300 years, Science China Earth Sciences, 52, 1172-1182, 10.1007/s11430-009-0118-8, 2009.

Yu, Z., Ciais, P., Piao, S., Houghton, R. A., Lu, C., Tian, H., Agathokleous, E., Kattel, G. R., Sitch, S., Goll, D., Yue, X., Walker, A., Friedlingstein, P., Jain, A. K., Liu, S., and Zhou, G.: Forest expansion dominates China's land carbon sink since 1980, Nat Commun, 13, 5374, 10.1038/s41467-022-32961-2, 2022.

Yu, Z., Jin, X., Miao, L., and Yang, X.: A historical reconstruction of cropland in China from 1900 to 2016, Earth System Science Data, 13, 3203-3218, 10.5194/essd-13-3203-2021, 2021.

Yue, C., Ciais, P., Houghton, R. A., and Nassikas, A. A.: Contribution of land use to the interannual variability of the land carbon cycle, Nature Communications, 11, 3170, 10.1038/s41467-020-16953-8, 2020.

Yue, C., Xu, M., Ciais, P., Tao, S., Shen, H., Chang, J., Li, W., Deng, L., He, J., Leng, Y., Li, Y., Wang, J., Xu, C., Zhang, H., Zhang, P., Zhang, L., Zhao, J., Zhu, L., and Piao, S.: Contributions of ecological restoration policies to China's land carbon balance, Nature Communications, 15, 9708, 10.1038/s41467-024-54100-9, 2024.

Zhao, C., He, F., Yang, F. and Li, S.: Uncertainties of global historical land use scenarios in past-millennium cropland reconstruction in China, Quaternary International, 641, 87-96, 10.1016/j.quaint.2022.03.020, 2022.

Zhu, Y., Xia, X., Canadell J., Piao, S., Lu, X., Mishra, U., Wang, X., Yuan, W., and Qin, Z.: China’s Carbon Sinks from Land-Use Change Underestimated. Nature Climate Change, 15, 4: 428-35, 2025.